UCRL 8860

UNIVERSITY OF CALIFORNIA

Ernest O. Lawrence

Radiation Laboratory

NUCLEAR-SPIN AND HYPERFINE-STRUCTURE MEASUREMENTS ON THE RADIOACTIVE IODINE AND ASTATINE ISOTOPES

TWO-WEEK LOAN COPY

This is a Library Circulating Copy which may be borrowed for two weeks. For a personal retention copy, call Tech. Info. Division, Ext. 5545

DISCLAIMER

This document was prepared as an account of work sponsored by the United States Government. While this document is believed to contain correct information, neither the United States Government nor any agency thereof, nor the Regents of the University of California, nor any of their employees, makes any warranty, express or implied, or assumes any legal responsibility for the accuracy, completeness, or usefulness of any information, apparatus, product, or process disclosed, or represents that its use would not infringe privately owned rights. Reference herein to any specific commercial product, process, or service by its trade name, trademark, manufacturer, or otherwise, does not necessarily constitute or imply its endorsement, recommendation, or favoring by the United States Government or any agency thereof, or the Regents of the University of California. The views and opinions of authors expressed herein do not necessarily state or reflect those of the United States Government or any agency thereof or the Regents of the University of California.

UCRL-8860
Physics and Mathematics

UNIVERSITY OF CALIFORNIA

Lawrence Radiation Laboratory
Berkeley, California

Contract No. W-7405-eng-48

NUCLEAR SPIN AND HYPERFINE-STRUCTURE MEASUREMENTS ON THE RADIOACTIVE-IODINE AND ASTATINE ISOTOPES

Hugh Leslie Garvin
(Thesis)

August 7, 1959

Printed for the U. S. Atomic Energy Commission

Printed in USA. Price $2.50. Available from the
Office of Technical Services
U. S. Department of Commerce
Washington 25, D.C.

NUCLEAR-SPIN AND HYPERFINE-STRUCTURE MEASUREMENTS ON THE RADIOACTIVE IODINE AND ASTATINE ISOTOPES

Contents

Abstract 4

I. Introduction 6

II. Theory of Nuclear-Spin and Hyperfine-Structure Measurements 12

A. Hyperfine Structure in Field-Free Region 12

B. Hyperfine Structure in Presence of External Magnetic Field 16

C. Nuclear-Spin Determination 20

D. Hyperfine-Structure Measurements 22

III. The Experimental Apparatus 27

A. The Vacuum System 27

B. The Magnet System 32

C. Beam Sources 33

D. Detector Systems 37

E. Radio-Frequency Systems 41

F. Radioactivity Decay Counters 46

IV. Sample Preparations 50

A. The Iodine Isotopes 50

B. Astatine-211 57

V. Results 60

A. Nuclear-Spin Measurements 60

B. Hyperfine-Structure Measurements 74

Contents (continued)

VI. Discussion of Results 82

A. Nuclear-Spin Results 82

B. Hyperfine-Structure Results 88

Acknowledgments 93

Appendix A. Identification of Isotopes 95

Appendix B. Previous Experimental Observations on Iodine and Astatine 106

Appendix C. Relativistic Correction Factors 109

References 110

NUCLEAR-SPIN AND HYPERFINE-STRUCTURE MEASUREMENTS ON THE RADIOACTIVE IODINE AND ASTATINE ISOTOPES

Hugh L. Garvin

Lawrence Radiation Laboratory, University of California, Berkeley, California

August 7, 1959

ABSTRACT

Atomic-beam magnetic-resonance techniques have been used to measure the nuclear spins of the following radioactive iodine and astatine isotopes:

Isotope	Half-life	Spin	Isotope	Half-life	Spin
I^{123}	13 hr	5/2	I^{132}	2.3 hr	4
I^{124}	4.5 days	2	I^{133}	21 hr	7/2
I^{126}	13 days	2	I^{135}	6.7 hr	7/2
I^{130}	12.5 hr	5	At^{211}	7.2 hr	9/2
I^{131}	8 days	7/2			

In addition, the magnetic-dipole interaction constant, a, and the electric-quadrupole interaction constant, b, for I^{131} and I^{132} were found to be:

$$a_{131} = 575.906 \pm 0.015 \text{ Mc/sec}$$

$$b_{131} = 578.849 \pm 0.120 \text{ Mc/sec}$$

$$a_{132} = \pm 566 \pm 5 \text{ Mc/sec}$$

$$b_{132} = \pm 67 \pm 36 \text{ Mc/sec.}$$

These interaction constants imply the following values of magnetic-dipole moment, μ, in nuclear magnetons (nm), and electric-quadrupole moment, Q, in centimeters squared (cm^2):

$$\mu_{131} = 2.738 \pm 0.001 \text{ nm}$$
$$Q_{131} = -0.412 \pm 0.020 \times 10^{-24} \text{ cm}^2$$
$$\mu_{132} = \pm 3.08 \pm 0.03 \text{ nm}$$
$$Q_{132} = \mp 0.048 \pm 0.025 \times 10^{-24} \text{ cm}^2.$$

The atomic-beam apparatus used to perform these measurements was especially designed for use with volatile radioactive samples. The magnetic-resonance signals were observed by collection of the radioactive-beam atoms on silver-plated buttons which were subsequently counted in low-background particle detectors.

The theory of the experimental method, the equipment used, and the sample-preparation techniques are described. A discussion is included of the interpretation of the results in light of the single-particle shell-model theory of nuclear structure.

I. INTRODUCTION

In recent years atomic-beam techniques have been used to determine certain properties of numerous atomic nuclei. Of particular significance is the measurement of nuclear spins (angular momenta) and electromagnetic multipole moments by this technique. These properties may be inferred from observations of optical spectra, from experiments using paramagnetic and nuclear-magnetic resonance techniques, and by analysis of the β and γ-ray decay properties of radioactive atoms. In these methods, however, the resolution is generally lower than that obtained in atomic-beam measurements or else the size of sample required is much larger. Thus atomic-beam investigations are of particular importance in observing the nuclear properties of radioactive atoms in samples as small as 10^{11} to 10^{13} atoms. In studying these nuclear properties, it is of interest, when possible, to make measurements on a series of isotopes of the same element, for in such a series the total nuclear charge (Z) is constant, and the variation in nuclear properties must be attributable to the variation in the number (N) of neutrons present. The radioactive iodine isotopes constitute such a series.

Experiments with atomic and molecular beams date back to 1911 when Dunoyer observed the distribution of neutral particles effusing with thermal energies from the orifice of a heated oven

chamber into an evacuated region.[1] In 1921 Stern and Gerlach demonstrated in a beam experiment the spatial quantization of atomic systems subjected to applied magnetic fields,[2] and in 1938 Rabi and collaborators refined the technique to observe resonance transitions between atomic hyperfine states.[3] Several treatises have been written recently which describe in detail the development of molecular-beam techniques and provide excellent references to present applications.[4-8]

The majority of the halogen isotopes lie in the mass regions where the collective effects in nuclear structure are not expected to dominate,[9-12] and thus the experimental evidence concerning these isotopes should serve to test the applicability of the single-particle shell model of the nucleus. Atomic-beam investigations of the properties of the stable halogen isotopes include the works of Davis, Feld, Zabel, and Zacharias on Cl^{35} and Cl^{37};[14] of King and Jaccarino on Br^{79} and Br^{81};[15] and of Jaccarino, King, and Stroke on I^{127}.[16] Concurrent with the radioactive iodine and astatine investigations reported herein, some radioactive bromine isotopes are being investigated and will be reported elsewhere.[17] Appendix B includes a survey of the measurements of the properties of iodine by optical and microwave spectroscopy and by analysis of the β and γ-ray decay schemes.

The particular atomic-beam magnetic-resonance technique used for many current investigations is the "flop-in" technique

proposed by Zacharias in 1942.[18] Since the measurements reported herein were made by this same method, a brief description of the technique is appropriate.

Figure 1 shows a schematic representation of the components used in a flop-in experiment. The beam is formed by collimation of the atoms that thermally effuse from the source chamber (O) into the main chamber which is evacuated by diffusion pumps. The pressure in this region is low enough that an atom or molecule admitted has only a small probability of collision with a molecule of the residual gases present, while traversing the length of the apparatus. Thus neutral particles are expected to travel in straight lines throughout the evacuated system until they collide with the walls unless their paths may be deflected by applied magnetic fields (A and B). Only a small portion (about 10^{-4} or 10^{-5}) of the total number of atoms that effuse from the source have their velocities directed approximately along the center line of the apparatus so that they travel to a detecting device (D) at the other end. The path of the atoms between the source and the detector passes between the pole pieces of three electromagnets: A, C, and B in that order. Magnets A and B provide strongly inhomogeneous fields with the gradients directed perpendicular to the beam direction and to the length of the source slit. If the beam atom has an effective magnetic dipole moment (due primarily to the electronic magnetic moment), the field gradient

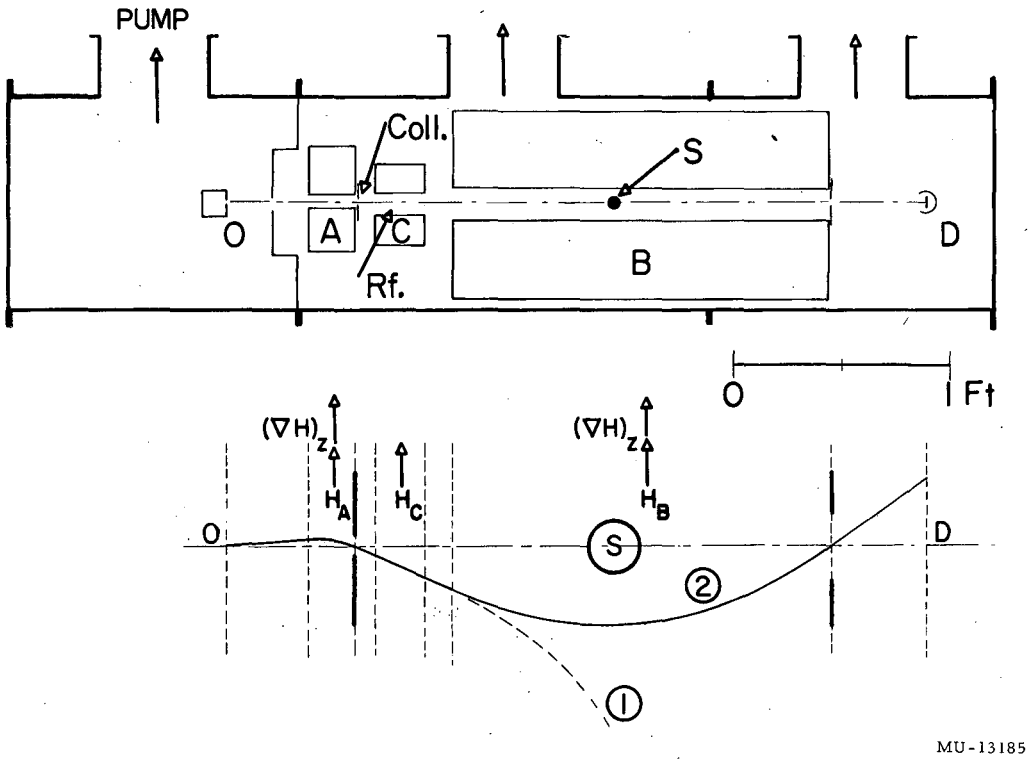

Fig. 1. Schematic arrangement and trajectory in an atomic-beam, flop-in apparatus.

produces a deflection of the atom that is proportional to this effective moment. If the gradients of the two magnets are oppositely directed, the deflection caused by the first magnet may be exactly counterbalanced by the second with the result that the atom reaches the detector by an S-shape path rather than by a straight line. But, when the magnets are arranged with their gradients in the same direction then an atom which has been deflected in the first magnet will continue to be further deflected by the second magnet (see trajectory 1 in Fig. 1) and will miss the detector. If, after the atom has been deflected by the first magnet, a transition is induced by a radio-frequency (rf) oscillating field which reverses the sign of its effective magnetic moment, then the atom will not be lost from the beam but be refocussed (see trajectory 2) onto the detector and recorded as a resonance signal. This reversal of atomic moment and resulting refocussing of the atoms of the beam is the basis of the "flop-in" technique.

In order to exclude background signal caused by molecules or high-velocity atoms present in the beam (since these particles are not sufficiently deflected by the magnetic fields to miss the detector), a stopwire (S) is inserted into the path of the beam. The atoms which have undergone the flop-in transition are deflected around this stopwire. Hence the flop-in method has the desirable feature that the detector signal is very low until the rf transition is induced and the

resonance signal is observed.

The quantization of angular momentum results in discrete magnetic states of the atom. The sign reversal in magnetic moment required for refocussing the atomic beam is accomplished by inducing transitions between two of these magnetic states. These transitions take place in the third field region, the C field, located between the deflecting magnets. The C field is homogeneous and generally weaker than the A and B fields. A small oscillating magnetic field is superimposed upon the homogeneous C field to produce a magnetic torque on the atom and cause transitions between magnetic states.[4] The magnitude of the static C field and the frequency of the oscillating field required for resonance transitions between discrete states are related to the nuclear properties of the atom as will be shown in the next section.

II. THEORY OF NUCLEAR-SPIN AND HYPERFINE-STRUCTURE MEASUREMENTS

A. Hyperfine Structure in Field-Free Region

The hyperfine energy level structure of an atom is due to the electromagnetic interaction between the nucleus and the electrons. This interaction is measured by the energy required to change the relative orientation of the nuclear and electronic angular momenta.

In the absence of external fields, the Hamiltonian describing the hyperfine interaction in terms of the angular-momentum operators ($\vec{I}$ for the nuclear and $\vec{J}$ for the electronic momenta*) is

$$\mathcal{H} = a\,(\vec{I} \cdot \vec{J}) + b\,Q_{op} + c\,O_{op} + \ldots \qquad (1)$$

where $(\vec{I} \cdot \vec{J})$, Q_{op}, and O_{op} are the operators for the magnetic-dipole, electric-quadrupole, and magnetic-octupole interactions, and a, b, and c are their respective proportionality

---

*The usual notation is used: $\overrightarrow{\text{angular momentum}} = \hbar\,\vec{I}$ or $\hbar\,\vec{J}$. The magnitude of the nuclear angular momentum, I, is referred to as the nuclear spin. Here $\hbar$ is $1/2\pi$ times Planck's constant, 6.6252×10^{-27} erg-sec. Nuclear and electronic magnetic moments are given by $\vec{\mu}_I = g_I \mu_o \vec{I}$ and $\vec{\mu}_J = g_J \mu_o \vec{J}$. The respective nuclear and electronic g factors are g_I and g_J ($g_I \cong \frac{1}{2000}\, g_J$), and μ_o, the Bohr magneton is 0.9273×10^{-20} erg/gauss.

constants. In this form the interaction is expressed in terms of successively higher multipole orders starting with the magnetic-dipole interaction.*

In field-free regions the total angular momentum, $\vec{F}$, is the vector sum of $\vec{I}$ and $\vec{J}$ such that $F = I + J$ where F, I, and J are the quantum numbers of these vectors and m_F, m_I, and m_J are their respective projections on a reference direction (usually taken as the direction of an applied field). In an (F , m_F) representation, neglecting configuration interactions, the matrix elements of the dipole operator are diagonal in F and are[5]

$$\langle F , m_F | (\vec{I} \cdot \vec{J}) | F, m_F \rangle = 1/2 \, [F(F+1)-J(J+1)-I(I+1)]. \qquad (2)$$

The Q_{op} term denotes the electric quadrupole interaction which arises from a nonspherical charge distribution of the nucleus in the presence of an electric field gradient due to the electronic configuration. Here too the operator is expressed in

---

*The highest possible moment that can be observed by atomic-beam methods is the 2^k moment where k is the smaller of 2I or 2J. Parity considerations exclude the electric multipole moments of odd-k order and magnetic moments of even-k order.

terms of $\vec{I}$ and $\vec{J}$[5, 19, 20] giving

$$Q_{op} = \frac{3\,(\vec{I}\cdot\vec{J})^2 + 3/2\,(\vec{I}\cdot\vec{J}) - I(I+1)J(J+1)}{2I(I-1)J(J-1)}. \tag{3}$$

The magnetic-octupole interaction, O_{op}, as shown by Schwartz[21] is

$$O_{op} = \frac{5\left\{(\vec{I}\cdot\vec{J})^3 + 4\,(\vec{I}\cdot\vec{J})^2 + 4/5\,(\vec{I}\cdot\vec{J})[-3I(I+1)J(J+1) + J(J+1) + 3] - 4I(I+1)J(J+1)\right\}}{4\,I(I-1)(2I-1)J(J-1)(2J-1)} \tag{4}$$

For a single non-s electron the magnetic-dipole-interaction constant, a, can be related to the nuclear magnetic moment, μ_I, and the electronic radial operator $\langle r^{-3}\rangle$ by

$$a = \frac{\mu_o^2}{h} g_I \frac{\mathcal{F} 2\ell(\ell+1)}{j\,(j+1)} \langle r^{-3}\rangle \tag{5}$$

as shown by Casimir.[22]

The electric quadrupole constant, b, was also evaluated by Casimir and, may be written

$$b = -\frac{e^2}{h} Q\mathcal{R} \frac{2\ell}{(2\ +3)} \langle r^{-3}\rangle \tag{6}$$

In these expressions we have $g_I = \frac{m}{M}\frac{\mu_I}{I}$, μ_I being the nuclear magnetic moment in nuclear magnetons, and Q is the nuclear electric quadrupole moment in units of $10^{-24}\,cm^2$.

The relativistic correction factors are $\mathcal{F}$ and $\mathcal{R}$. For

iodine; we have

$\mathcal{F} = 1.061$ and $\mathcal{R} = 1.128$ (see Appendix C). The other terms have their usual meanings:

μ_0, the Bohr magneton = 0.9273×10^{-20} ergs/gauss,

h, Planck's constant = 6.625×10^{-27} erg-sec,

e, the charge on the electron = 4.803×10^{-10} e.s.u.,

ℓ and j, the electronic orbital and total angular momenta (for iodine, $\ell = 1$, $j = 3/2$),*

$\langle r^{-3} \rangle$, the expectation value of the radial operator,

m, the mass of the electron = $9.1085(6) \times 10^{-28}$ gm,

and N, the mass of the proton = $1.67243(10) \times 10^{-24}$ gm.

The solutions of Eq. (1) for given values of I and J in an (F, m_F) representation are the energies of the hyperfine levels. These are denoted by W_F, where F takes on values between the maximum of $(I+J)$ and the minimum of $(J-I)$ when $J \geqslant I$ or $(I-J)$ when $I \geqslant J$. The frequency separations of two such levels, $\Delta\nu$ (e.g., $\Delta\nu_{12}$ between F_1 and F_2 or $\Delta\nu_{23}$ between F_2 and F_3), obtained by using Eqs. (2), (3), and (4), are

---

*The halogen atoms each have one electron missing from the noble-gas configuration. Hund's rules predict a $^2P_{3/2}$ atomic ground state which has been confirmed spectroscopically.[23] The separation of the $^2P_{3/2}$ and $^2P_{1/2}$ levels has been observed to be 7603 cm^{-1}.[24]

$$\Delta\nu_{12} = \frac{a}{2} \quad (C_1 - C_2) + b\ (Q_{op1} - Q_{op2})$$

$$\Delta\nu_{23} = \frac{a}{2} \quad (C_2 - C_3) + b\ (Q_{op2} - Q_{op3}), \tag{7}$$

where we have $C = [F\ (F+1) - J\ (J+1) - I\ (I+1)]$, and the octupole interaction is neglected. Thus the measurement of two such separations provides unique solutions for the values of a and b.

B. Hyperfine Structure in Presence of External Magnetic Field

When an external magnetic field is applied to the atomic system, the energy of interaction of the nucleus and the electrons with the field must be included, and the Hamiltonian becomes

$$\mathcal{H} = a\ (\vec{I}\cdot\vec{J}) + b\ Q_{op} - g_J \mu_o \vec{J}\cdot\vec{H}_o - g_I \mu_o \vec{I}\cdot\vec{H}_o\ , \tag{8}$$

where the minus signs are consistent with the definitions in Section A.

Figure 2 illustrates the energy-level diagram appropriate to this Hamiltonian for the case where $J = 3/2$, $I = 7/2$, and $b/a = 1.005$ (as for iodine-131). At the extreme left in Fig. 2, when the applied field is zero, the energy levels, W_F, are just those of the hyperfine structure discussed in Section A.

The application of a small magnetic field, H_o, splits the hyperfine levels into components which may be labelled by

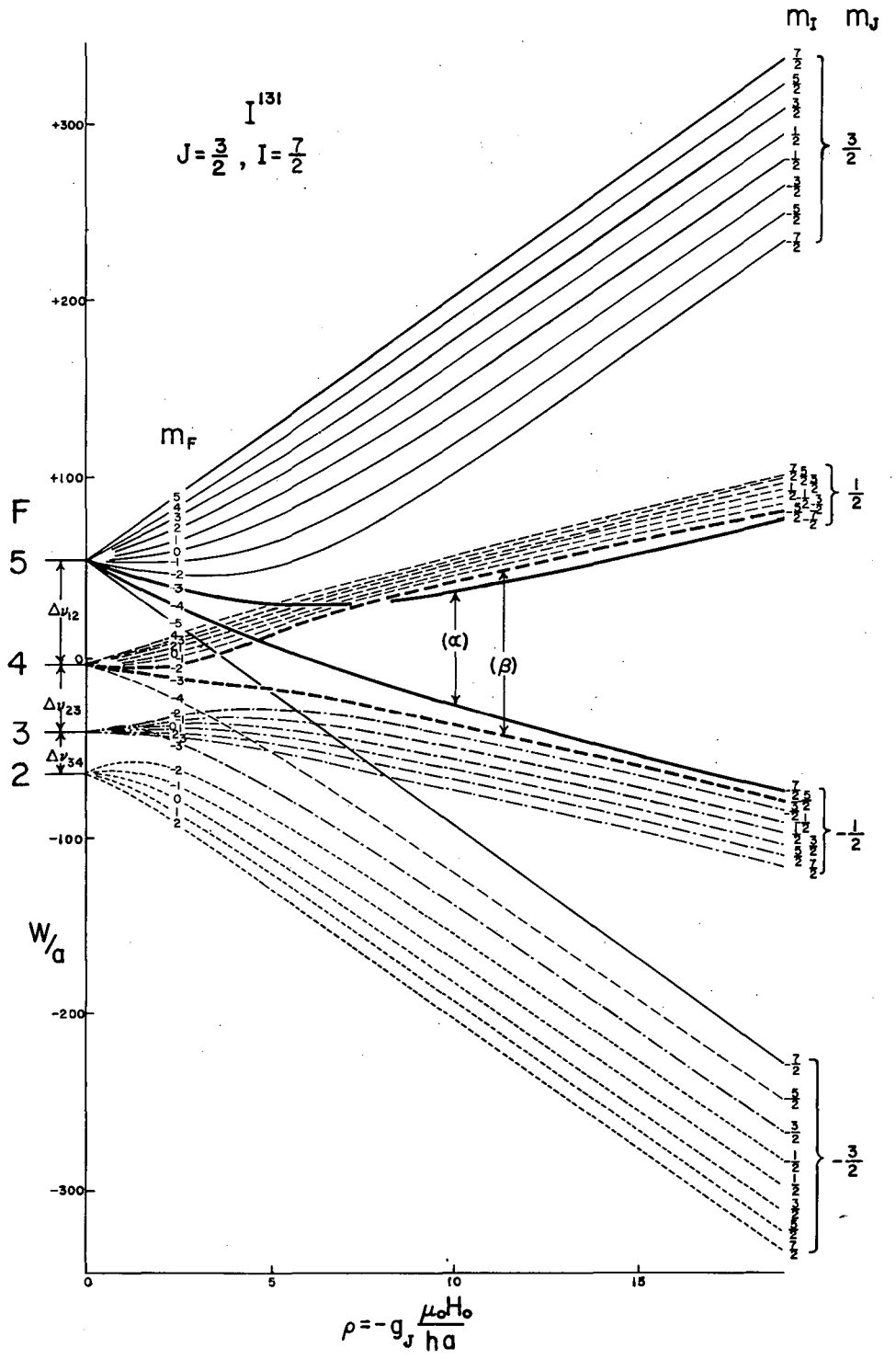

Fig. 2. Energy-level diagram for I^{131}.

m_F, the projection of F on the field direction. At low field values (e.g., between 0 and 30 gauss) the splitting is essentially linear, (the Zeeman region) and if we neglect off-diagonal elements in $\mathcal{H}$, the energy of each component is given to a good approximation by[7]

$$W_{F,m_F} = W_F - m_F\, g_F\, \mu_0 H_0. \tag{9}$$

Where g_F is defined by

$$g_F = g_J \frac{F(F+1) + J(J+1) - I(I+1)}{2F(F+1)} + g_I \frac{F(F+1) + I(I+1) - J(J+1)}{2F(F+1)}. \tag{10}$$

Figure 3a shows a pictorial representation of the manner in which $\vec{I}$ and $\vec{J}$ couple to form a resultant $\vec{F}$ which precesses in a weak magnetic field. At higher field values, however, when the interaction of $\vec{J}$ with the field is comparable to or greater than the interaction between $\vec{I}$ and $\vec{J}$ (see Fig. 3b), then the nondiagonal terms in $\vec{F}$ in the matrix equations can no longer be neglected and the Hamiltonian must be solved exactly to determine the values of the energy levels which are depicted in Fig. 2. An IBM-653 computer has been programmed to facilitate the solution. A complete description of the method of solution is given elsewhere.[25-27]

Electromagnetic theory[28] predicts that an atomic system may transfer from one of the magnetic hyperfine states to another upon the absorption or emission of the proper multipole

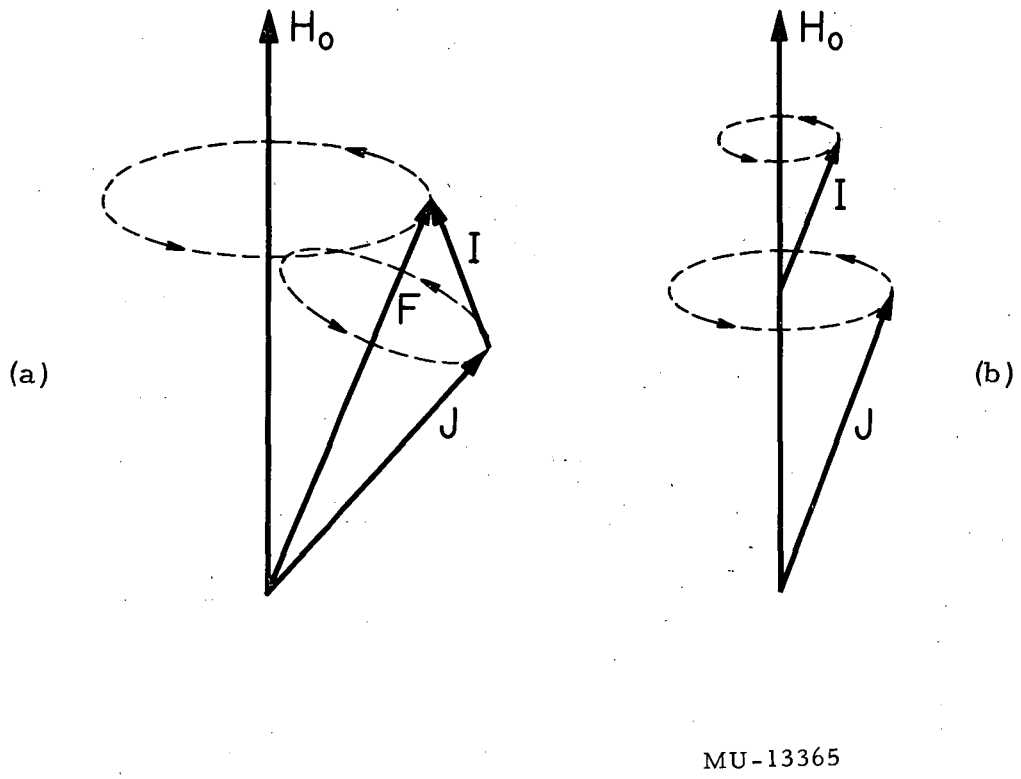

Fig. 3. Precession of $\vec{I}$, $\vec{J}$, and $\vec{F}$ in (a) a weak and (b) a strong magnetic field.

radiation. In atomic-beam magnetic-resonance experiments, transitions are induced by means of magnetic dipole radiation and the transitions allowed obey the selection rules:

$$\Delta F = \pm 1 \text{ or } 0$$

$$\Delta m_F = \pm 1 \text{ or } 0.$$

For an atom to undergo a transition and reach the detector as a flop-in resonance, the projection, m_J, of $\vec{J}$ on the field direction must change from + 1/2 to - 1/2 or vice versa. Examination of the level diagram shows that in only two cases can this condition (plus the selection rules) be satisfied for two levels within the same F state. These two transitions may be denoted α and β. For J = 3/2 (I > 0) and normal (numerically consecutive) ordering of the F levels,* these are:

$$\begin{aligned} \alpha &: (F=I+3/2,\ m_F = -I+1/2) \longleftrightarrow (F=I+3/2,\ m_F = -I-1/2) \\ \beta &: (F=I+1/2,\ m_F = -I+3/2) \longleftrightarrow (F=I+1/2,\ m_F = -I+1/2). \end{aligned} \tag{11}$$

C. Nuclear Spin Determination

In the weak field region, Eq. (9) gives the energy difference between two levels with $\Delta F = 0$ and $\Delta m_F = \pm 1$ as

---

*Cases have been found (e.g., in the hyperfine structure of Br^{76}, see Garvin et al.[29] where the quadrupole interaction is large enough to cause an inversion of F levels. When this occurs additional flop-in resonances may be allowed.

$$\Delta W(m_F = \pm 1) = g_F \mu_o H_o, \tag{12}$$

or as a frequency of transition

$$\nu(\Delta m_F = \pm 1) = g_F \frac{\mu_o H_o}{h}.$$

Using the fact that g_I is much less than g_J, Eq. (10) may be approximated by $g_F = g_J \dfrac{F(F+1)+J(J+1)-I(I+1)}{2F(F+1)}$. (10')

The nuclear spin, I, will be integral for nuclei with even atomic number, A = Z+N, and half-integral for nuclei with odd A. Thus, for given values of g_J, F, and J, Eq. (10') indicates that g_F will take on only the discrete values associated with I. At a known value of H_o, the observation of the flop-in α and β resonance frequencies for an isotope determines its value of g_F and thus its nuclear spin.

The value of the magnetic field is measured by observing a flop-in resonance of a calibration beam of atoms (e.g., of potassium or cesium) whose g_F is well known. From Eq. (12), we have

$$\nu_K = g_{F_K} \frac{\mu_o H_o}{h}$$

and

$$\nu_{\alpha \text{ or } \beta} = g_{F_{\alpha \text{ or } \beta}} \frac{\mu_o H_o}{h}.$$

Dividing these, we obtain

$$\frac{\nu_{\alpha \text{ or } \beta}}{\nu_K} = \frac{g_{F_{\alpha \text{ or } \beta}}}{g_{F_K}} \tag{13}$$

so that at a particular field setting the spin may be determined by comparing the rf frequencies at which the resonances occur in the sample beam and in the calibration beam.

The halogen atomic-beam apparatus has a resonance line width of approximately 0.1 Mc at low C field values.* Consequently, in this weak field range, high-spin resonances may not be separated enough for resolution. In order to determine the value of the spin unequivocally, α and β spin resonances are observed at several values of the magnetic field where the resonances are resolved. This procedure was used for the measurement of the nuclear spins of iodine-123, -124, -126, -130, -131, -132, -133, -135, and astatine-211.

D. Hyperfine-Structure Measurements

The best values of the interaction constants, a and b, are obtained by the direct observation of the zero-field hyperfine separations by inducing $\Delta F = \pm 1$ transitions. Before a search for the direct transitions is undertaken, however, it is advisable that good estimates for hyperfine separations be obtained. (For some stable isotopes the zero-field hyperfine

---

*The resonance line width is due primarily to inhomogeneity of the C field and the characteristics of the rf loop which induces the transitions.

structure may be inferred from spectroscopic analysis, but this is seldom the case for radioactive isotopes).

In order to obtain good estimates of the $\Delta\nu$ values, the α and β resonances are observed at successively higher field values until shifts from the frequencies predicted by Eq. (12) are observed. These shifts may be related to the $\Delta\nu$ values by a pertubation calculation to second order in H_o which gives

$$\delta\nu_\alpha^{(2)} = \frac{2}{3}\,\frac{I^2}{I+1}\,\frac{1}{\Delta\nu_{12}}\,\nu_o^2 \tag{14a}$$

for the shift in the α resonance, and

$$\delta\nu_\beta^{(2)} = \left[\frac{(2I+1)^2\,(2I+3)^2}{(2I+9)^2}\right] \times \left[\frac{-6I(I-1)}{(I+1)(2I+3)^2}\,\frac{1}{\Delta\nu_{12}} + \frac{2(2I+3)(2I-1)(I-1)}{I(I+1)(2I+1)^2\,\Delta\nu_{23}}\right]\nu_o^2 \tag{14b}$$

for the shift in the β resonance. This calculation was made for $J = 3/2$ and $I > 1/2$. The $\Delta\nu$ values are defined as

$$\Delta\nu_{12} = W(F = I + 3/2) - W(F = I + 1/2)$$

and

$$\Delta\nu_{23} = W(F = I + 1/2) - W(F = I - 1/2),$$

and ν_o refers to the frequency predicted by Eq. (12). Clearly

a calculation to higher order in H_o is required for shifts in the β resonance if I = 1.

The values of $\Delta\nu_{12}$ and $\Delta\nu_{23}$ from the pertubation calculations may not be precise enough to permit a search for the direct transitions, but they do give preliminary values of a and b by Eq. (7). For better values, the IBM-653 program must be used to solve the Hamiltonian exactly.[27] The program starts with the preliminary values of a and b and calculates the theoretical transition frequencies to be expected at C field settings where resonances were actually observed. It then performs a χ^2 test* of the closeness of fit of the theoretical and observed frequencies.[30] The parameters a and b are then changed within the program until the best fit of the theoretical to observed frequencies is obtained. Resonances are then observed at higher fields, and the results are added to the previous information until the uncertainties in a and b are small enough that $\Delta\nu_{12}$ and $\Delta\nu_{23}$ can be predicted accurately and the search for the direct transitions can be undertaken. This procedure was followed in the determination of the nuclear moments of I^{131} and I^{132}.

---

*As applied in this case χ^2 is $\sum_{i=1}^{N} \frac{(f^i_{observed} - f^i_{theoretical})^2}{(\text{uncertainty of measurement})_i^2}$ where each value of i refers to a particular observation.

The observation of $\Delta\nu_{12}$ and $\Delta\nu_{23}$ determines the values of a and b by Eq. (7). The constants a and b are in turn related to μ_I and Q by Eqs. (5) and (6). In these equations, however, the value of $\langle r^{-3} \rangle$ is not known precisely, because of the uncertainty in values of the electronic wave functions, therefore the values of μ_I and Q are calculated in an alternate manner proposed by Davis, Feld, Zabel, and Zacharias.[14]

For two isotopes of the same element, $\langle r^{-3} \rangle$ will be the same; thus it is possible to relate the constants of two such isotopes by

$$\frac{a_1}{a_2} = \frac{g_{I_1}}{g_{I_2}} = \frac{\mu_1 I_2}{\mu_2 I_1}. \tag{15}$$

The value of μ for I^{127} was measured by Walchi by direct comparison to the moment of the proton in a nuclear magnetic resonance experiment,[31] and the interaction constants a_{127}, b_{127}, and c_{127} were measured in an atomic-beam experiment by King and Jaccarino.[16] Therefore the value of μ for any other iodine isotope may be directly related to μ_{127} by use of Eq. (15). Furthermore, on eliminating $\langle r^{-3} \rangle$ from Eqs. (5) and (6), one obtains

$$\frac{a_1}{b_1} = \frac{-\mu_0^2}{e^2} \frac{\mathcal{F}}{\mathcal{R}} \frac{(\ell+1)(2\ell+3)}{j\,(j+1)} \frac{g_{I_1}}{Q_1} \tag{16}$$

or

$$Q_1 = -\frac{\mu_0^2}{e^2} \frac{\mathcal{F}}{\mathcal{R}} \frac{(\ell+1)(2\ell+3)}{j\,(j+1)} \frac{b_1\, g_{I_1}}{a_1}.$$

Again, using Eq. (15) to substitute for a_1, the value of Q for any iodine isotope may be related through its b value to the measured value of μ_{127}. The value of Q determined by Eq. (16) represents the experimentally observed value of the quadrupole moment. This value differs from the true quadrupole moment of the nucleus by a factor C, the Sternheimer correction for the deformation of the electronic charge distribution due to the nonspherical nuclear charge distribution.[32, 33] For iodine, Q of Eq. (16) must be multiplied by $C = 1.029$.

III. EXPERIMENTAL APPARATUS

A. The Vacuum System

The atomic-beam apparatus used for the work reported herein was especially designed for use with volatile radioactive materials. Although the theory of operation and basic components are the same as those described earlier,[34, 35, 36] the apparatus is unique in some of its design features. As shown in Figs. 4 and 5 the machine has essentially an "inside-out" construction in that the A, B, and C magnets are mounted external to the vacuum system. This manner of construction has certain advantages: (1) apparatus alignment is easily performed, (2) sections may be removed for repair or replacement with little disturbance of the rest of the system, (3) the C field region is accessible for insertion and modification of the rf loops, (4) the C field magnet pole pieces are easily adjusted to vary the resonance line width, (5) the component parts may be readily decontaminated or replaced (if this should become necessary because of accumulation of long-lived radioactive material).

The oven and detector chambers are brass cans which are mounted approximately 30 inches apart astride Dural runners. Three smaller vacuum chambers span the distance between the oven and the detector can and provide the low-pressure region through which the beam passes. In the early stages of

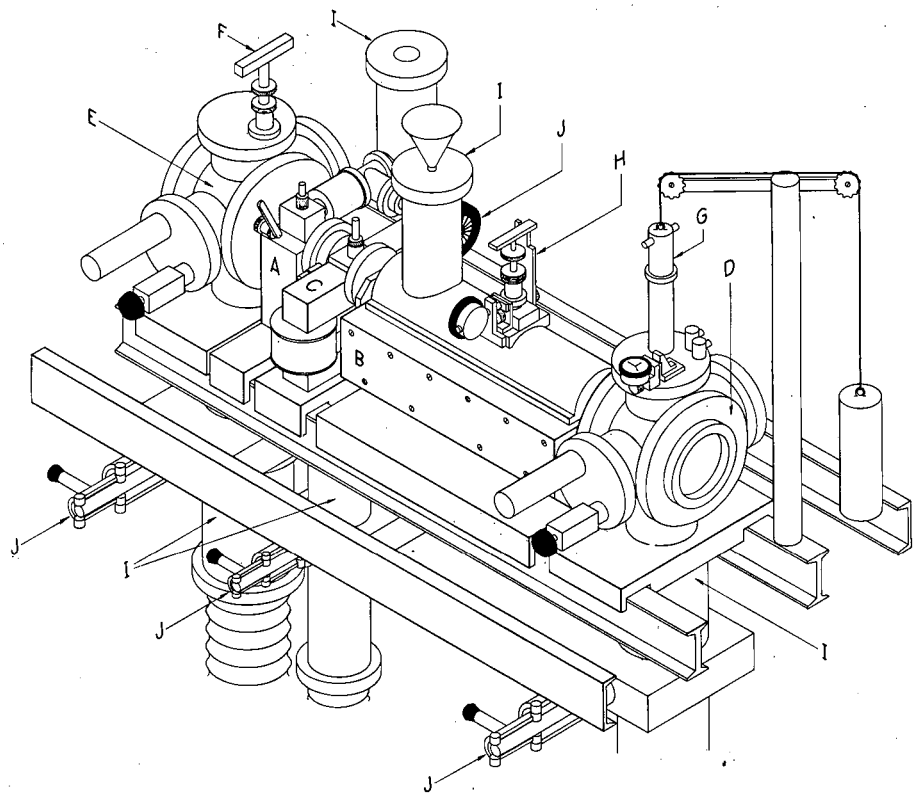

MU-13930

Fig. 4. Schematic view of the atomic-beam apparatus. A, B, C - magnets; D - detector can; E - oven can; F - calibrating oven; G - button loader; H - stopwire assembly; I - liquid-nitrogen traps; J - valves.

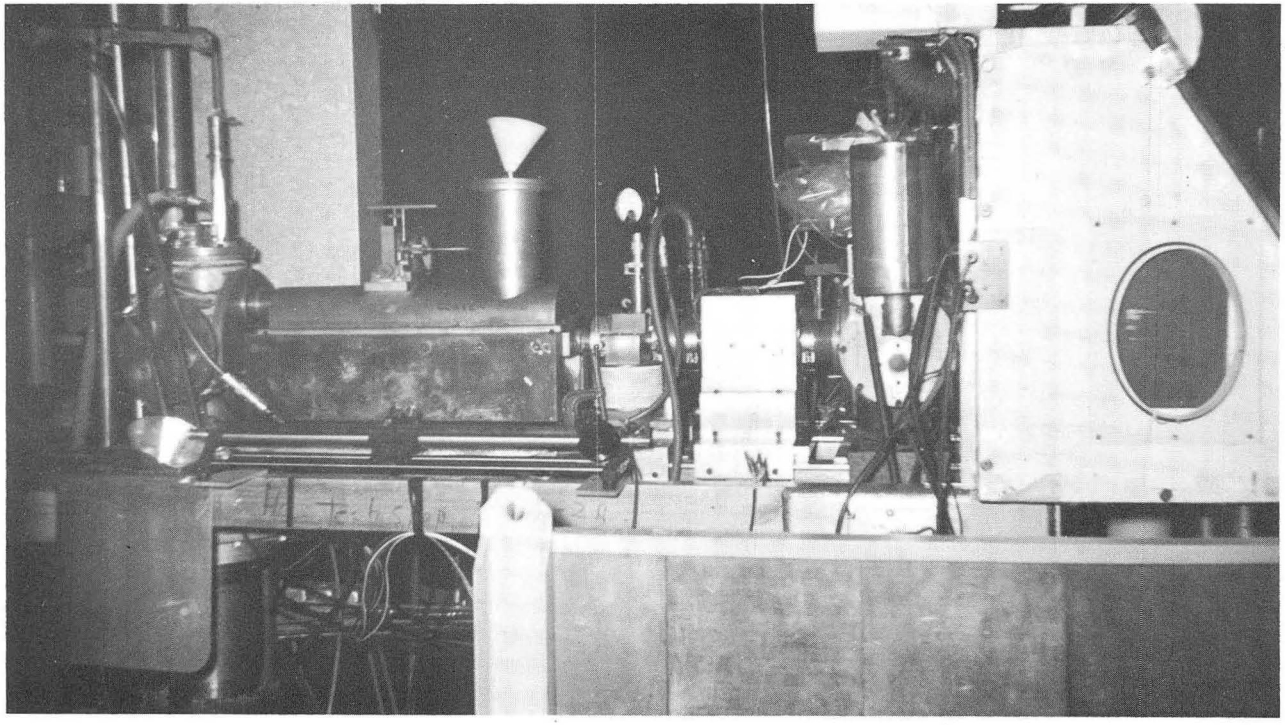

ZN-2213

Fig. 5. The atomic-beam apparatus.

construction, stainless steel tubes of 0.080 in. and 0.375 in. diam. were passed between the A and B magnet gaps in order to carry the beam. However it was found that only extremely weak beams would reach the detector through these tubes, and it became necessary to surround the A and B magnet gaps by manifolds which were pumped separately. Thus the pumping takes place through the long slot between the pole tips (see Fig. 6). The C field chamber is a rectangular box with the pole tips externally mounted. In this box are mounted the rf-loop assembly and the collimating slits, which are adjustable by micrometer screws from outside the vacuum chamber.

The oven and detector chamber are evacuated by MCF 700 oil-diffusion pumps.* The A field manifold and the C field regions are each pumped by MCF 300 pumps; the B field manifold is evacuated by a 2-in. pumping tube into the detector chamber. Rapid- action vacuum valves are included in each pumping line above the liquid-nitrogen traps. These valves allow the vacuum system to be brought up to atmospheric pressure for repair or modification without cooling the pumps or warming the traps.

---

*The MCF series of pumps is manufactured by Consolidated Vacuum Corp., Rochester, N. Y., a subsidiary of Consolidated Electrodynamics, Inc. The Temescal valves employed in the system are produced by the same company.

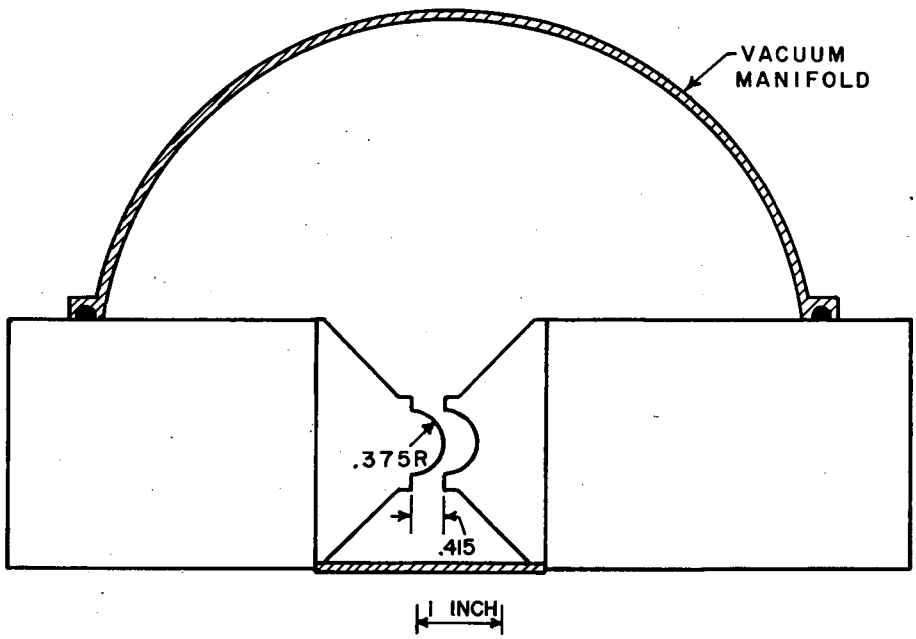

CROSS SECTION B POLE TIPS

MU-18036

Fig. 6. B - Magnet cross section with vacuum manifold.

The system can be pumped from atmospheric pressure to 3×10^{-6} mm Hg in approximately 5 minutes.

The solid angle of the beam reaching the detector is determined primarily by the detector-can entry slits (0.100 in. wide) and the collimating slits (0.042 in. wide). As noted in the Introduction, a stopwire serves to intercept fast atoms or molecules which are not deflected by the A and B magnets; it is located at the position of maximum beam deflection in the B magnet. In this apparatus, the stopwire is a blade with cross sectional dimensions 0.052 in. by 0.100 in. which can be rotated to intercept more or less than the geometric beam width (0.072 in.) It can be adjusted laterally in the beam or withdrawn completely from the path of the beam. A small background signal may be detected due to beam atoms which are deflected around the stopwire by small-angle scattering off of the residual gases. Therefore the collimator slits, instead of being set to the geometric width determined by the solid angle formed by the source slit and the detector width, are set slightly narrower to reduce this signal.

B. The Magnet System

The A and B magnets used for beam deflection are similar to those described in earlier literature.[36] They are 2-1/2 in. and 21-1/4 in. long respectively and constructed of Armco iron. Fig. 6 shows the cross section of the B magnet pole tips which

produce the inhomogeneous deflecting field. The A magnet is similar in design but reduced in size. The A magnet has a gap of 0.100 in. with maximum field of 6000 gauss and field gradient of about 30,000 gauss/cm. The B magnet produces approximately the same field, but has a gap of 0.415 in. and field gradient of about 7,200 gauss/cm. These magnets are energized by wire-wound coils of approximately 1200 turns each, and the current (1.8 to 4.0 amp) is provided by an adjustable 300-v regulated supply (stable to 1 part in 30,000). The details of the chopper amplifier and current-regulation system are described in the thesis of Gilbert Brink.[36]

The C field-magnet pole pieces are 2-in.-long (along the beam) and 1-1/2-in.-high. Two coils of approximately 1500 turns each energize this magnet to fields strengths of 0 to 1200 gauss. The current (0 to 20 ma) was originally provided by 6-v wet-cell batteries, but when measurements were to be made at high field values (requiring 300 ma), it became necessary to incorporate a DC current-regulating supply. This supply uses a Delco 2N174 transistor as a current-control element and a Kintel Model 111BF high-gain amplifier to regulate the current. The stability is one part in 10^5.

C. Beam Sources

The majority of atomic-beam experiments use a heated-oven system from which the sample effuses to form the beam.

Such an oven is used to produce the potassium or cesium calibration beam in the present apparatus. The calibration oven is constructed on the end of a shaft that extends down into the top of the oven chamber. As the oven is heated by a small nichrome heater to such a temperature that the vapor pressure of the potassium increases to approximately 0.5 mm of Hg, the atoms of potassium effuse from the 0.003- by-0.040-in. source slit to form the beam.*

At room temperature, the vapor pressure of iodine (0.3 mm of Hg) is sufficient for beam production. Therefore the iodine sample is attached externally to the apparatus and allowed to diffuse into the apparatus through glass tubing; Iodine vapor is primarily diatomic molecules (I_2) and it is necessary to dissociate these molecules to form the atomic beam. The molecules are dissociated by (a) an rf discharge which is maintained in the quartz tube containing the 0.005- by-0.030-in. source slit (see Fig. 7), or by (b) thermal dissociation within a platinum tube heated to approximately 900°C (see Fig. 8). Either technique produces a beam of 80 to 90% atomic iodine. The second technique was found more desirable to use because

---

*For a narrow-slit source of atoms, the pressure within the oven must be low enough that the mean free path is greater than the width of the slit [the Knudsen condition].[37]

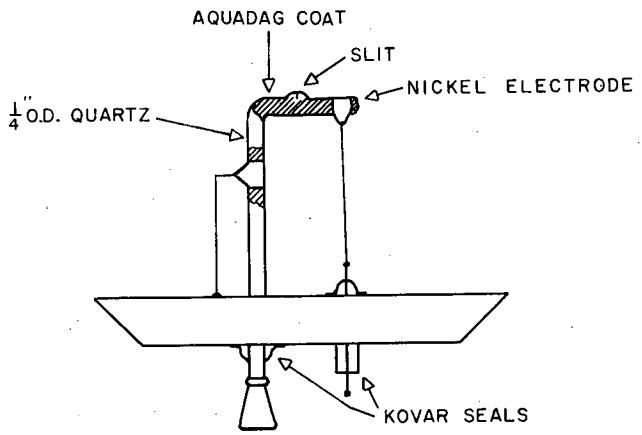

RF DISCHARGE TUBE

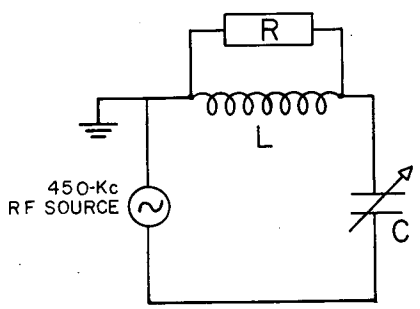

DISCHARGE STABILIZER

MU-14243

Fig. 7. Radio-frequency discharge tube and discharge-stabilizing circuit.

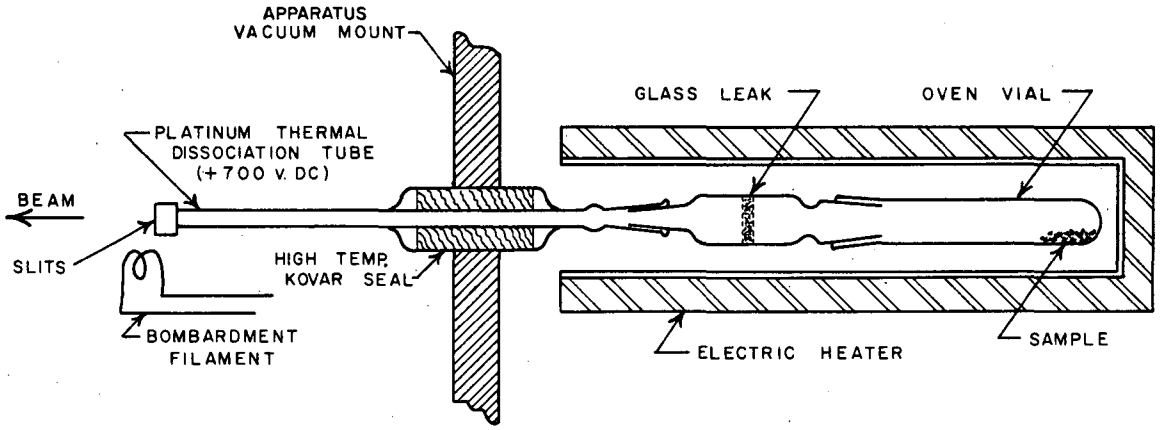

ASTATINE BEAM SOURCE

MU-15447

Fig. 8. Platinum thermal-dissociation beam source.

the electrical discharge causes a deposit in the quartz tube which frequently clogs the wire-drawn slit opening. The production of a beam of atomic astatine requires special techniques, which will be discussed in Chapter IV.

The radioactive sample is attached externally to the atomic-beam machine in a Berkeley-type glove box (see Figs. 5 and 9). The oven end of the apparatus is sealed into this box, and the box is closed and vented through a radioactive filter system. The box affords protection to the operator when handling samples and also permits safe removal of one type of source assembly and insertion of another without exposure of the apparatus interior to the room.

Metallic potassium or cesium may be used interchangeably for the calibration beam. Due to the comparatively low hyperfine structure of potassium as well as its low spin value, 3/2, its frequency of resonance transition increases much more rapidly than for cesium as the C field is increased. Thus it becomes awkward to use for high-field studies. However, the potassium metal is easier and safer to handle than cesium. Therefore, it is used for the majority of low-field measurements, and cesium is used only when high-field resonances are to be observed.

D. Detector Systems

The alkali calibration beam is detected by surface

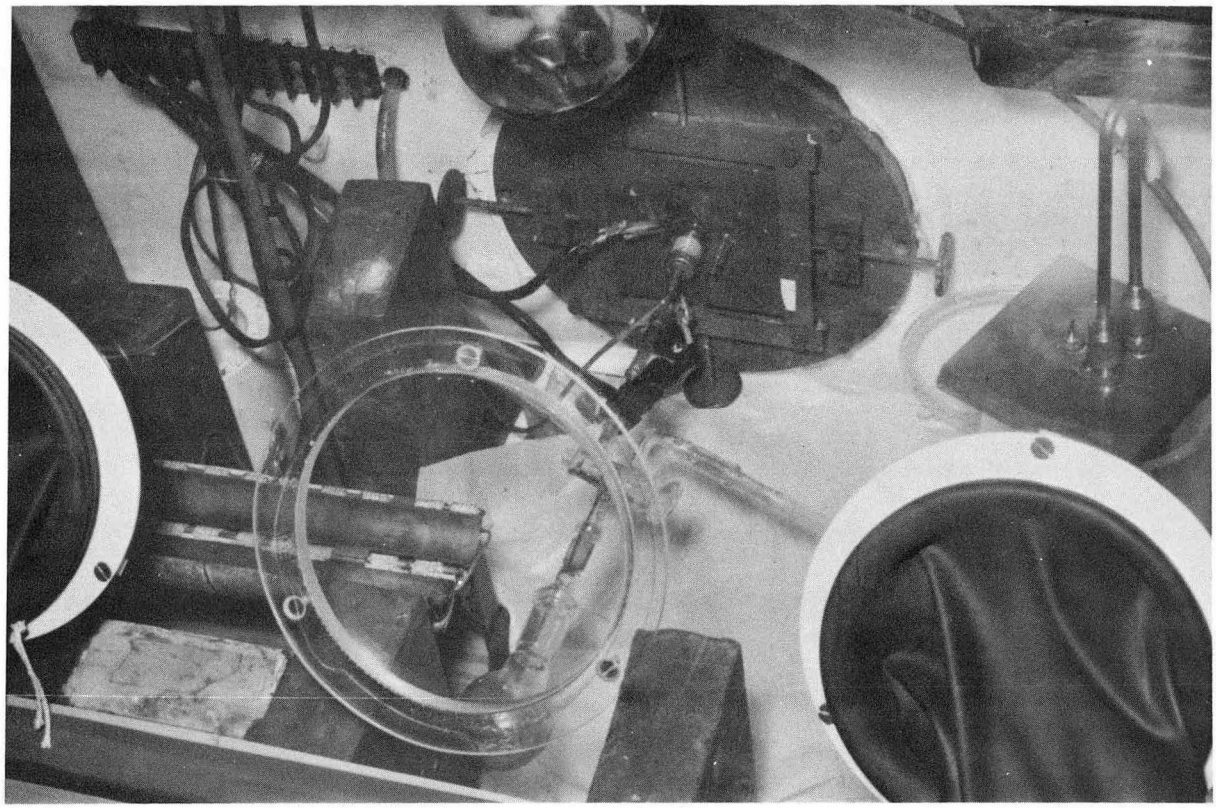

ZN-2212

Fig. 9. Sample vial attached to atomic-beam apparatus.

ionization of the beam atoms on a heated tungsten ribbon. The positive ion current of 10^{-12} to 10^{-9} amps is amplified by a vibrating-reed electrometer (Applied Physics Corp., Pasadena; Model 31) and displayed on a Speedomax recorder.

The radioactive beam is detected by allowing the beam atoms to fall upon small metallic buttons (see Fig. 10) which are inserted into the vacuum system. The size of the beam signal is determined by detection of the radioactive decay of the atoms deposited. The buttons are coated with a suitable surface for efficient collection of the beam atoms.* In the case of the halogens, early experiments showed that freshly vacuum-plated silver surfaces are the most efficient and reproducible for collection. It was noted that electroplated silver surfaces are only about half as efficient as vacuum-plated, and that the efficiency of collection of the silver surface decreases by a factor of about four when the buttons are exposed to air for 15 hr. Thus, it is necessary to store freshly coated buttons in vacuum jars until ready for use.

---

*Refer to the work on the radioactive rubidium and gallium isotopes.[38, 39] A recent survey has also been made of the characteristics of atomic deposition.[40]

ZN-2210

Fig. 10. Cyclotron target holder; tellurium target foil; collection buttons for the radioactive atomic beam.

E. Radio-Frequency Systems

The transitions induced between atomic hyperfine states are brought about by the superposition of an oscillating magnetic field on the static homogeneous C field. The atomic system is changed between magnetic substates by the change in magnetic torque produced by the superimposed static and oscillating fields.[5] For α or β resonances, the frequencies of transition may be in the range of 100 kc to 500 Mc, whereas for the direct transitions ($\Delta F = \pm 1$, $\Delta m_F = 0$ or ± 1), the frequencies will be of the order of the hyperfine splittings of the atom, which for I^{131} are greater than 2000 Mc. It is apparant, therefore, that a wide range of signal-generating equipment is required. Figure 11 shows the equipment used in performing these measurements and Table I identifies the models and their operating ranges. Since one frequency is required for the calibration of the C field and another for the sample transition, some frequency ranges of equipment are duplicated. The oscillators provide the signals which are fed to the rf loop through coaxial switches.

In order to observe resonances of the radioactive beam, the rf input is first set to the desired frequency of potassium resonance, then the C field is adjusted so that a resonance is observed. The calibration oven is removed from the line of the beam, the sample frequency is fed into the rf loop, the button

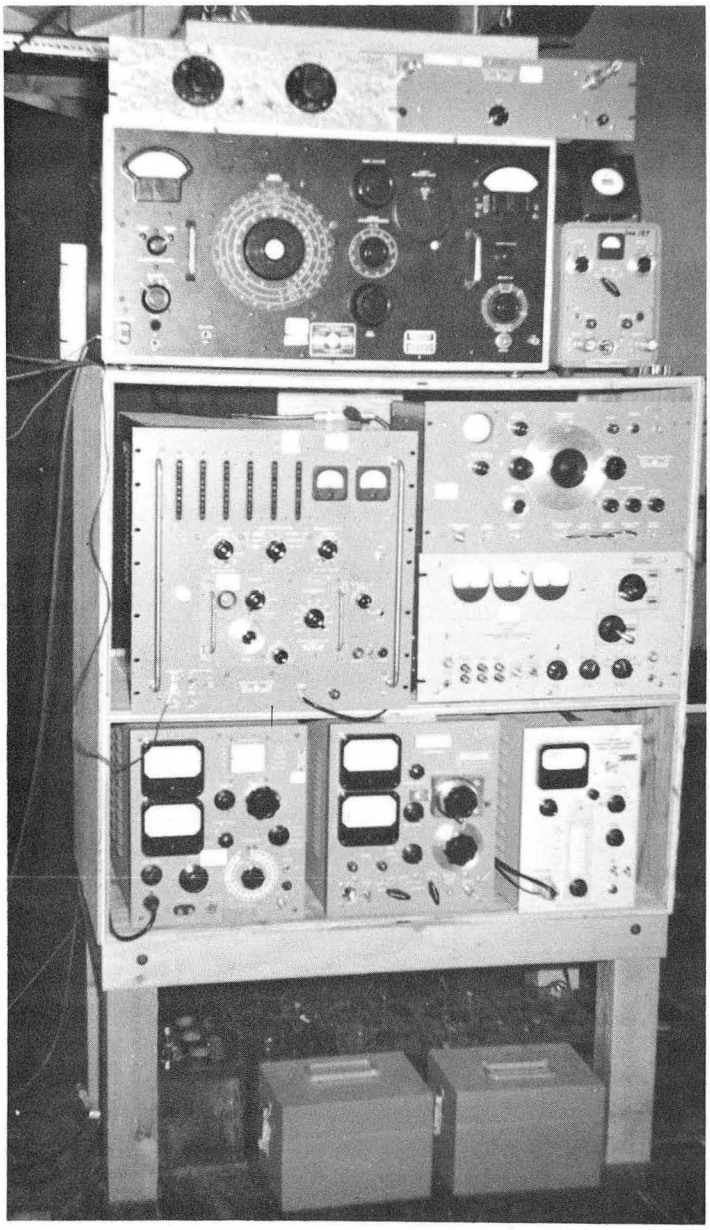

ZN-2209

Fig. 11. Radio-frequency equipment.

Table I

Radio-frequency equipment	
Model	Frequency range (Mc/sec)
Oscillators	
General Radio 805-C	0.100 to 50
Tektronix Type 190	0.350 to 50
Hewlett Packard 608 A	10 to 500
Hewlett Packard 612 A	450 to 1250
Airborne Instruments Lab. Type 124 C	220 to 2500
Amplifiers	
Hewlett Packard 460 A wide-band amplifier	0.500 to 180
Hewlett Packard 491 A, wave-tube amplifier	2000 to 4000
Other equipment	
Hewlett Packard 524 B frequency counter	
Bird Electronic Corp. 718 coaxial switches	

is inserted, and the exposure is started. After the desired exposure time (usually 5 to 10 min), the button is removed for counting, the calibrating oven is lowered into the line of the beam and the calibration frequency is again applied. If the magnetic fields have not changed in value the resonance of potassium will still appear. If the apparatus is no longer set to resonance, then the field must have drifted during the time of the exposure, so the exposure must be repeated. The stability of the magnet-current regulators is such that field drifts are observed only infrequently.

The frequencies are measured by a Hewlett-Packard Model-524B frequency counter which is accurate to 1 part in 10^6 by comparison with the signal output of the Atomichron (cesium-beam atomic clock).

The oscillating magnetic field is caused by rf current flowing in a loop device within the C field region. Simple hairpins of wire are sufficient at low frequencies to provide the rf signal required for resonance observation. However, for the wide frequency range involved in these experiments, a more efficient loop was developed. As shown in Fig. 12, the loop is essentially a section of shorted 50-ohm coaxial line. The dimensions are kept small for maximum influence of the rf current on the beam atoms. By the use of this loop, resonances in the 5- to 10-Mc range were easily observed with less than 10 milliwatts of rf power. The loop is dual-purpose in design,

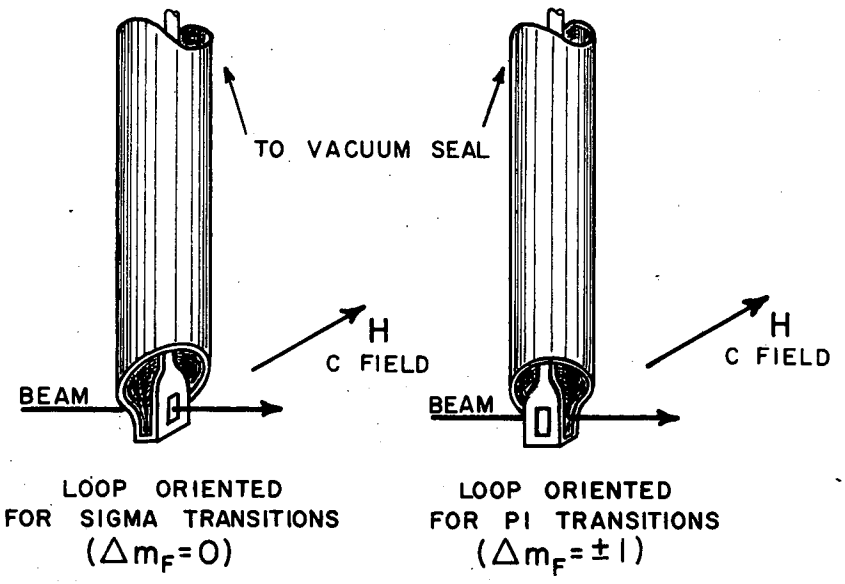

DUAL PURPOSE RF LOOP

MU-18042

Fig. 12. Dual-purpose radio-frequency loop.

since the selection rules allow two types of transitions: (a) Pi transitions ($\Delta m_F = \pm 1$) are caused by oscillating components of the rf field in directions perpendicular to the C field. (b) Sigma transitions ($\Delta m_F = 0$) are caused by oscillating components of the rf field in the direction parallel to the C field. The dual-purpose loop may be rotated to enhance the type of transition required.

F. Radioactivity Decay Counters

After deposition of the atomic beam on the sample buttons, specially designed counters are used to detect the decay products of the isotopes studied. Two types of counters are used: x-ray counters and α- or β-particle counters (shown in Fig. 13). The x-ray counters are thin-crystal scintillation counters.[41] A NaI crystal is used which is just slightly larger in area than the collecting surface of the button and is approximately 1/16-in.-thick. The crystal is mounted directly onto the surface of a 5819 photomultiplier tube inside of a 3-in. lead shield. An alignment hole serves to hold the button in close proximity to the crystal for counting. Amplified scintillation pulses from the phototube are registered in a single-channel pulse-height analyzer which is set to count the K x-rays associated with the electron-capture decay.

In cases where the sample isotope decays by α- or β-particle emission, continuous-flow methane proportional counters

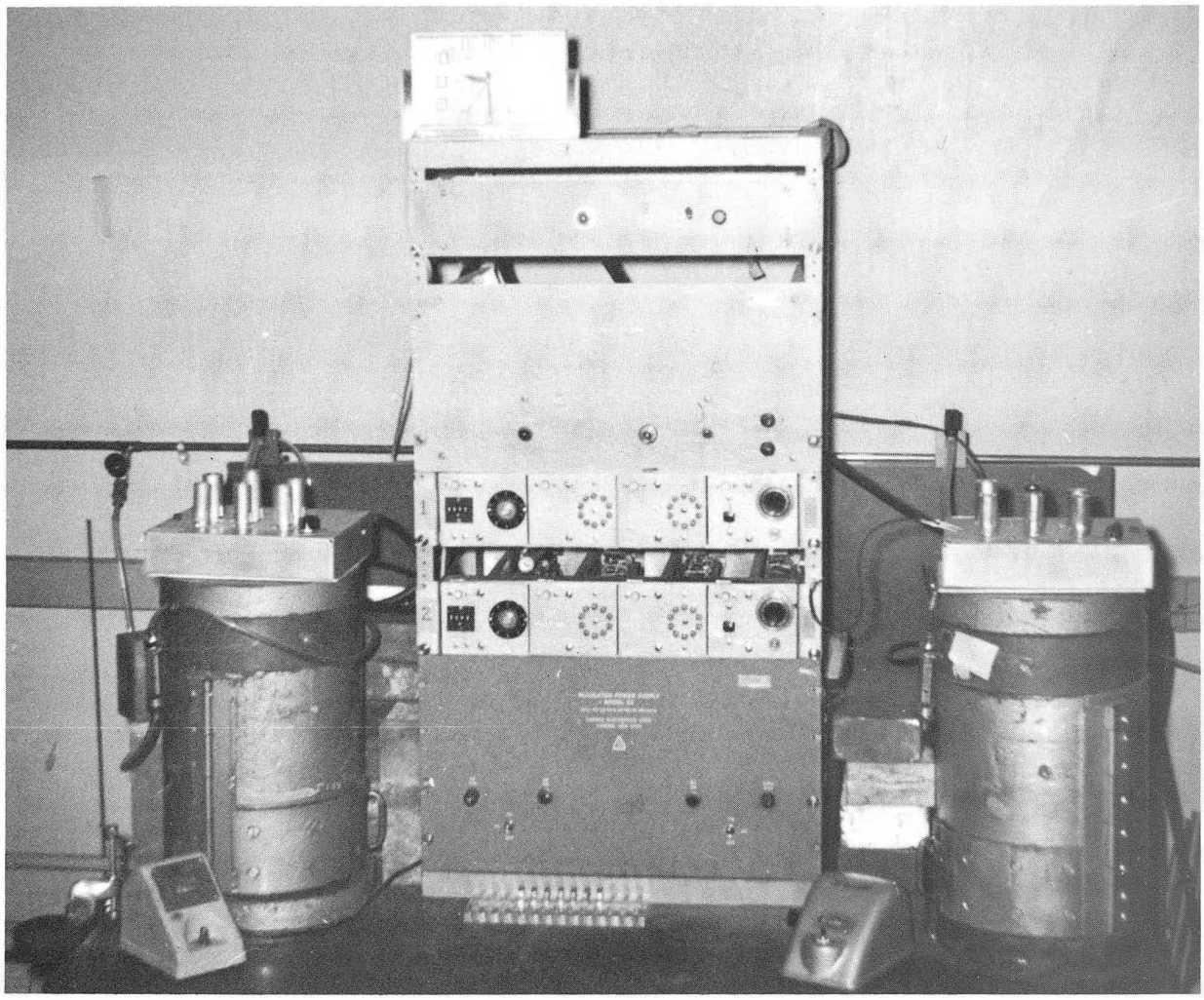

ZN-2214

Fig. 13. Radioactive decay counters.

are used. The volume of the ionization chamber of each counter is approximately 1 cu. in. (see Fig. 14), and the button is held approximately 1/4 in. from the high-voltage element, which is a 0.001-in. wire loop approximately 1/4 in. in diameter. The proportional counters are operated at 2800 v for detecting β-particles and have 1 to 3 counts/min. background. For α-counting, the voltage may be decreased to 2400 v and the background is thereby reduced to less than 1 count/min., with no appreciable loss in counting efficiency. The background in the x-ray counters is typically 0.5 to 2 counts per minute.

For analysis of decay half lives, a printing timer* was incorporated with the scaling units to record the time when a preset number of decay pulses has occurred. In cases where half-life analysis alone is not sufficient for isotope identification (see Appendix A), a 100-channel pulse-height analyser** was used in conjunction with a 1-1/2-in. crystal scintillation counter for identification of the characteristic gamma rays emitted.

---

*Clary Model-1920 printing timer; Clary Corp., San Gabriel, California.

**Penco Model PA-3; Pacific Electro-Nuclear Co., Culver City, California.

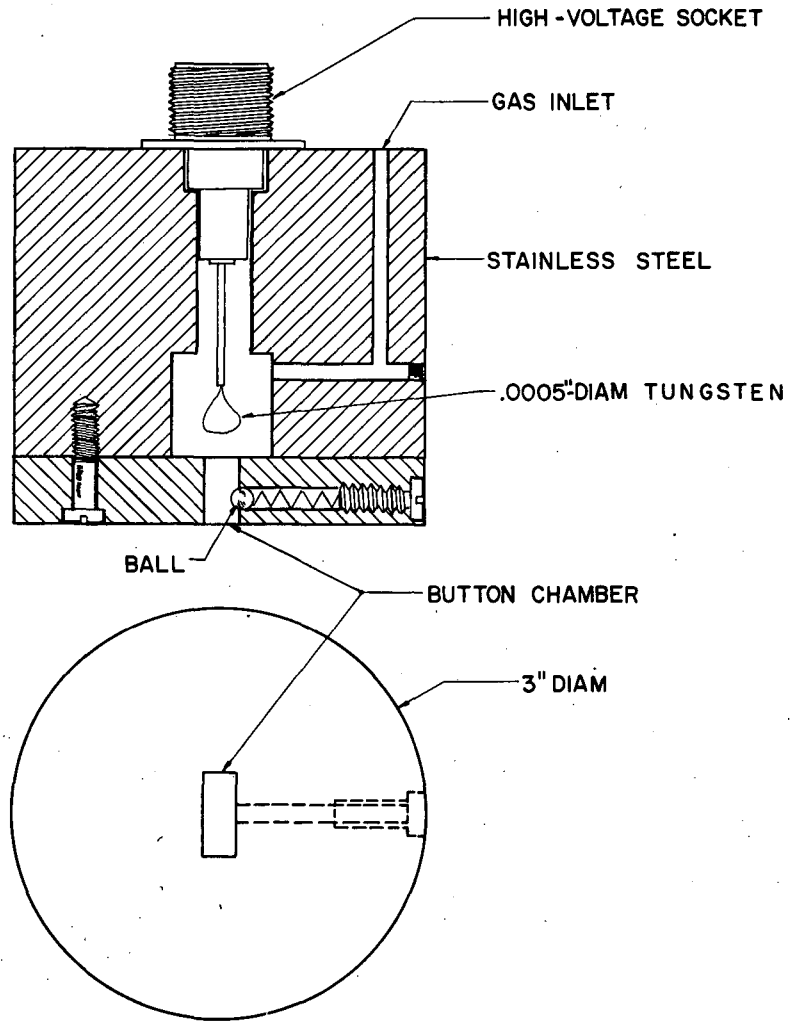

MU-17401

Fig. 14. Cross-section view of the continuous-flow proportional counters.

IV. SAMPLE PREPARATION

A. The Iodine Isotopes

The iodine isotopes which were studied in this investigation covered the mass range from 123 to 135. Because of this wide range no single technique of production could be used for all isotopes. The production techniques used were as follows:

Isotope	Manner of Production
$I^{123, 124}$	Alpha bombardment (with 48-Mev α particles) of powdered antimony metal, by the use of the (α, kn) reaction, where k = 1, 2, and 3.
$I^{126, 130}$	Proton bombardment (with 12-Mev protons) of tellurium metal melted onto an aluminum foil.
I^{131}	Purchased from Oak Ridge National Laboratories where it was separated as a reactor fission product.
I^{132}	Obtained by milking process from Te^{132} in an iodine generator provided by Brookhaven National Laboratory.

Isotope	Manner of Production
I^{133}	Purchased from Brookhaven where it was separated as a reactor fission product.
I^{132} through I^{135}	Produced in the fission of uranium-238 foils by 24-Mev deuteron bombardment.

All of the bombardments listed were performed in the Berkeley 60-in. cyclotron.

The basic objective in making an observable beam of any of the above isotopes is to separate the active isotope from the target material and mix it thoroughly with natural-iodine carrier in elemental form for admission into the beam apparatus. The total amount of radioactive sample is only 10^{12} or 10^{13} atoms, whereas the effusion rate of atoms into the apparatus is approximately 10^{14} atoms per second. Therefore it is necessary to mix the active sample with a natural carrier which lends stability to the beam and governs the running time of the sample.

Each isotope required the development of a chemical separation method peculiar to that isotope. In general the following three conditions should be satisfied: (a) The separation must be fast enough for observation of the desired isotope when short half-lives are involved, (b) It must be performed with safety against the possibility of radioactive dispersal and (c) It must also expose the researcher to a minimum amount of

radiation. The following sections describe the chemical techniques used for the iodine isotopes. Figure 15 shows the Berkeley-type glove box in which these chemical separations were performed.

1. I^{131} and I^{133}

Iodine-131 (8-day) and-133 (21-hr) were obtained from the Oak Ridge and Brookhaven National Laboratories as NaI in aqueous solution. The solution was made slightly acidic with H_2SO_4 and then $NaNO_2$ solution added. This oxidized the iodine to its elemental form, which is readily extracted into CS_2. The natural-iodine carrier (also dissolved in CS_2) is then added and mixed thoroughly with the radioactive iodine. The CS_2 is evaporated off, leaving crystals of iodine in the sample vial which is then attached directly to the beam machine. At room temperature it was found that iodine diffuses into the apparatus through the source slit at approximately 22 mg per hr. By the use of this fact the amount of iodine carrier is adjusted to give a convenient running time of the sample. The running time may be chosen appropriate to (a) the quantity of active material present, (b) the size of the beam desired, and (c) the half-life of the active sample. In order to illustrate these points, I^{131} and I^{133} were originally shipped as 100-millicurie (mC) samples (1 mC = 3.7×10^7 disintegrations (disint.) per sec). By the time the sample was received and the chemical

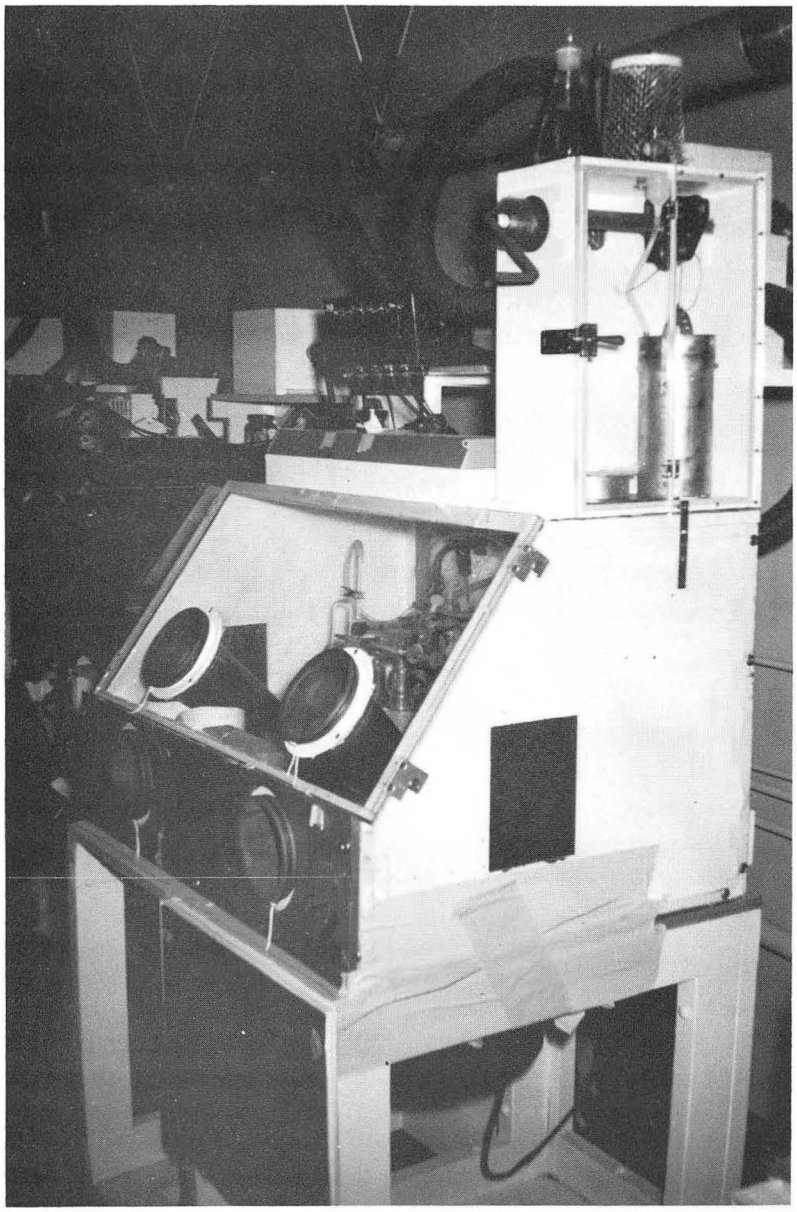

ZN-2211

Fig. 15. Berkeley-type chemistry box with the I^{132} generator attached (upper right).

separation was performed, the total sample had decayed to approximately 60 mC (thus the total sample was decaying at $\sim 2.2 \times 10^9$ disint./sec = 12×10^{10} disint./min). A convenient size of full beam counting rate is 500 counts/min. for each minute of button exposure (giving 2000 counts/min. for a 4-min. exposure; the resonance flop-in signal will be of the order of 2 to 4% of this full beam). If we assume a loss of a factor of 3 for counter solid angle and efficiency as well as button collection efficiency, the full beam reaching the button should be 1500 disint./min. The transmission of the apparatus is approximately 0.5×10^{-5}; therefore the total rate of effusion of active atoms should be such that they give approximately 3×10^8 disint./min. If the total sample were to effuse at this rate, it would last for $13 \times 10^{10} / 3 \times 10^8 = 430$ minutes = 7 hours. Thus the active-iodine sample was mixed with approximately 150 mg of natural-iodine carrier. The numbers used in the example are consistent with observed counting rates. In this example it was assumed that the half-life of the activity is long compared to the running time of the experiment. If the half-life is short, the amount of carrier is reduced to allow for the decay of the full beam during the time of the run.

2. <u>I^{123} and I^{124}</u>

I^{123} and I^{124} were produced by the α bombardment of powdered antimony metal. In order to remove the active iodine,

the target material was dissolved in hydrochloric acid (with H_2O_2 added to yield nascent chlorine). When the solution was made basic with sodium hydroxide, SbOCl was precipitated, and the solution containing the active iodine was filtered off. The solution was made acidic with H_2SO_4 and the iodine oxidized and extracted in the same way as I^{131}. In order to observe the 13-hr I^{123}, the sample was run immediately; however, for the 4.5-day I^{124}, the target was allowed to decay for 2 days to allow the I^{123} to die out with respect to the I^{124} before the separation was performed.

3. I^{126} and I^{130}

In order to reach the mass range 126 to 130, it was necessary to bombard the tellurium isotopes occurring naturally in this range and use the (p,n) reaction. Tellurium metal was melted onto a 0.025-in.-thick aluminum plate for bombardment. This plate was then covered with a 0.001-in. aluminum foil and clamped in a cyclotron target block (see Fig. 10). During bombardment the sample was cooled from the front by flowing helium gas and from behind by flowing water. These precautions were necessary to prevent overheating of the target and loss of Te and active iodine into the target chamber of the 60-in. cyclotron.

For separation of the iodine, the Te was dissolved in HNO_3 then the solution was made basic with concentrated NaOH.

When formic acid was added, the Te was precipitated and removed as TeO_2 and the iodine could be extracted as above. The separation of iodine from the Te target is approximately 80% efficient. A faster but less efficient (about 60%) technique of separation uses an evaporation system (see description under At^{211}) wherein the target Te is heated to approximately 700°C. The iodine is evolved and collected on a cooled platinum disc, which is subsequently washed in NaOH, from which the iodine extracted.

4. I^{132}

The 2.3-hr I^{132} is conveniently obtained by a "milking" process from 77-hr Te^{132} in an iodine generator provided by Brookhaven National Laboratory.[42] The Te is adsorbed in an alumina mesh within the generator and the iodine is removed by flushing with 25 ml of 0.01 M NH_4OH solution. The generator regains its secular equilibrium in approximately 12 hr, and fresh samples of I^{132} may be removed at 12-hr intervals if desired. Figure 15 shows the cupula on the Berkeley box which allows the generator to be flushed directly into the glove box for chemical processing.

5. $I^{132} \longrightarrow I^{135}$

The iodine isotopes I^{131} through I^{135} are produced as fission products when uranium-238 is bombarded with 24-Mev. deuterons. As described in sections 1 and 4 above, I^{131}, I^{132}, and I^{133} are obtained more economically, therefore deuteron

bombardments were only used to study I^{134} and I^{135}. Following bombardment, the uranium is dissolved in HCl. The solution is diluted with water, and then $NaNO_2$ is added to oxidize the iodine. The extraction into CS_2 efficiently separates the halogens from the other fission products.

B. Astatine-211

In 1940 Corson, Mackenzie, and Segrè isolated a radioactive element whose chemical, physical, and nuclear properties established it to be element 85, the last of the halogen group.[43] This element, which does not possess a stable isotope, was named astatine.[44] The measurement of the nuclear spin of the 7.2-hr At^{211} by an atomic-beam experiment constitutes the first direct spin determination of an isotope (with no stable counterpart) whose half-life is measured in hours.

The At^{211} was produced by an (α, 2n) reaction on a bismuth target in the Berkeley 60-in. cyclotron. A bombarding energy of 29 Mev was employed to produce preferentially At^{211} free at At^{210}. The astatine was separated from the target by an evaporation technique proposed by Barton, Ghiorso, and Perlman;[45] the target is heated to 700° C in air within a stainless steel crucible (see Fig. 16). The top of the crucible is closed by a water-cooled cylinder to which is clamped a platinum disc which serves to collect the astatine.

In order to produce an atomic beam, it was found necessary

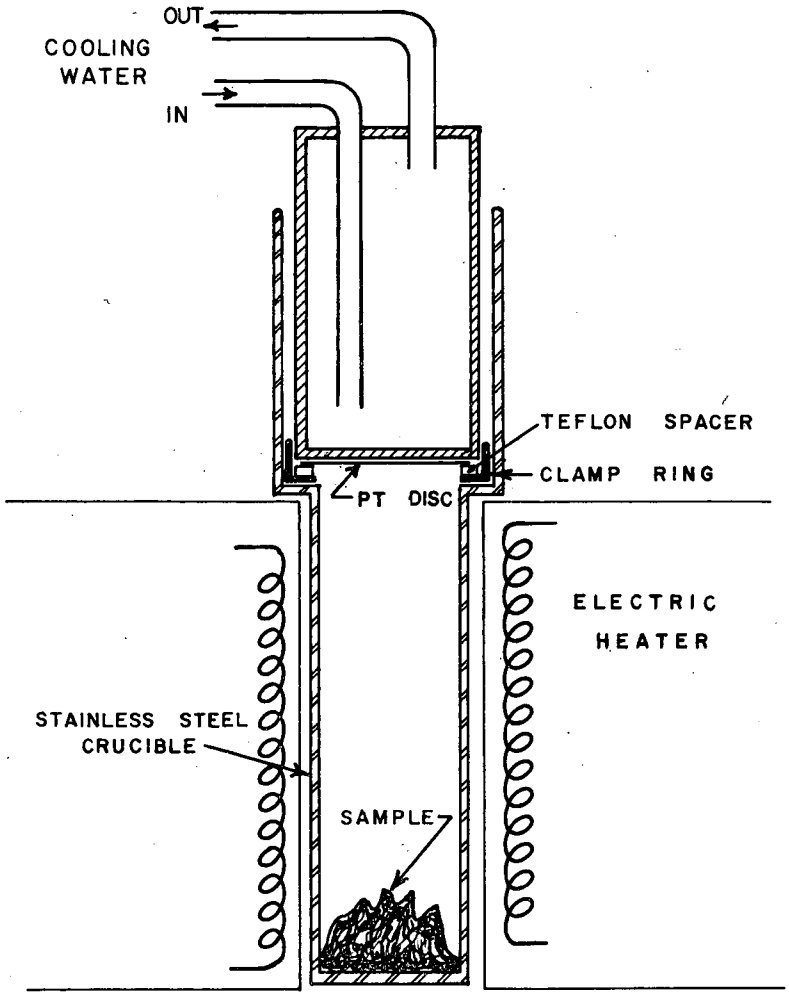

ASTATINE SEPARATION BOILER

MU-18037

Fig. 16. Cross-section view of the astatine separation boiler.

to mix the astatine with a natural carrier. Iodine was chosen because of the similarity of its chemical properties to these of astatine. The platinum foil was placed in an evacuated flask with approximately 150 mg of iodine and heated to drive off the astatine. An intimate mixing of the astatine and iodine was ensured by distilling the mixture several times from one end of the vial to the other. The atomic beam was produced by thermal dissociation of the I-At complex in the platinum source tube described in Chapter III.

It was found necessary to maintain the oven vial and associated glassware at a temperature of approximately 100°C to prevent adsorption of the active material onto the glass. The flow rate of the I-At mixture into the platinum tube was controlled by a slow leak made by partially fusing a fritted-glass filter. Despite the intimate mixing of iodine and astatine, the beam was not steady, and varied irregularly with time. In order to compensate for this variation, the resonance-button signals were normalized against the direct beam (i.e., the signal with the apparatus stop wire withdrawn), measured immediately before and after the resonance exposure.

In all of the sample preparations, when the radiation fields due to the sample were too high for separation in the standard glove box, the operations were performed by the use of remote manipulators in 2-in lead-shielded chemistry boxes.

V. RESULTS

A. Nuclear-Spin Measurements

The results of the spin measurements performed on the isotopes of iodine and astatine are summarized in Table II and have been published by the author in collaboration with T. M. Green, E. Lipworth and W. A. Nierenberg.[46-50] Magnetic-field values are listed at which resonances were observed and the type of flop-in resonance observed is given in parenthesis. The values of the spins of I^{125}, I^{127}, I^{128}, and I^{129}, which were measured elsewhere, are included for reference.

Figure 17 shows the spin search made on a sample containing I^{123} and I^{124}. The high signals at frequencies appropriate to spin 5/2 (α) and 5/2 (β) were decayed and attributable to 13-hr I^{123}. The signal at spin 2(α) was found to decay much more slowly, and was identified as being due to 4.5-day I^{124} (see Appendix A). Figure 18 shows the results of a similar search performed on a sample containing 13-day I^{126} (spin 2) and 12.5-hr I^{130} (spin 5).

Figure 19 shows the results of a spin search performed on a sample containing 2.3-hr I^{132}. Since this is essentially a pure isotope, only the resonances at spin 4 (α) and 4 (β) were detected.

Figures 20 through 28 show complete α and β rf resonances observed for the isotopes in Table II.

Table II

Results of spin measurements			
Isotope	Half life	Nuclear spin	Magnetic field at resonance (gauss)
I^{123}	13 hr	5/2	8.55(α, β); 17.07(α, β); 28.37(α, β)
I^{124}	4 day	2	8.55(α, β); 17.07(α, β); 28.37(α, β)
I^{126}	13 day	2	0.71(α, β); 1.42(α, β); 6.92(α, β)
I^{130}	12.6 hr	5	2.86(α, β); 8.56(α, β); 14.24(α, β)
I^{131}	8 day	7/2	see Table III
I^{132}	2.3 hr	4	2.82(α, β); 6.92(α, β);13.42(α, β)
I^{133}	21 hr	7/2	2.82(α, β); 6.92(α, β); 13.42(α, β)
I^{135}	6.7 hr	7/2	2.82(α, β); 6.92(α, β); 10.87(α, β)
At^{211}	7.2 hr	9/2	2.86(α, β); 5.71(α, β); 8.56(α, β)
Measurements made elsewhere:			
I^{125}	60 day	5/2	NMR[62]
I^{127}	stable	5/2	NMR[31]
I^{128}	25 min	1	Atomic beam[59, 61]
I^{129}	$> 10^7$ yr	7/2	NMR[31]
I^{130}	12.6 hr	5	Atomic Beam[61]

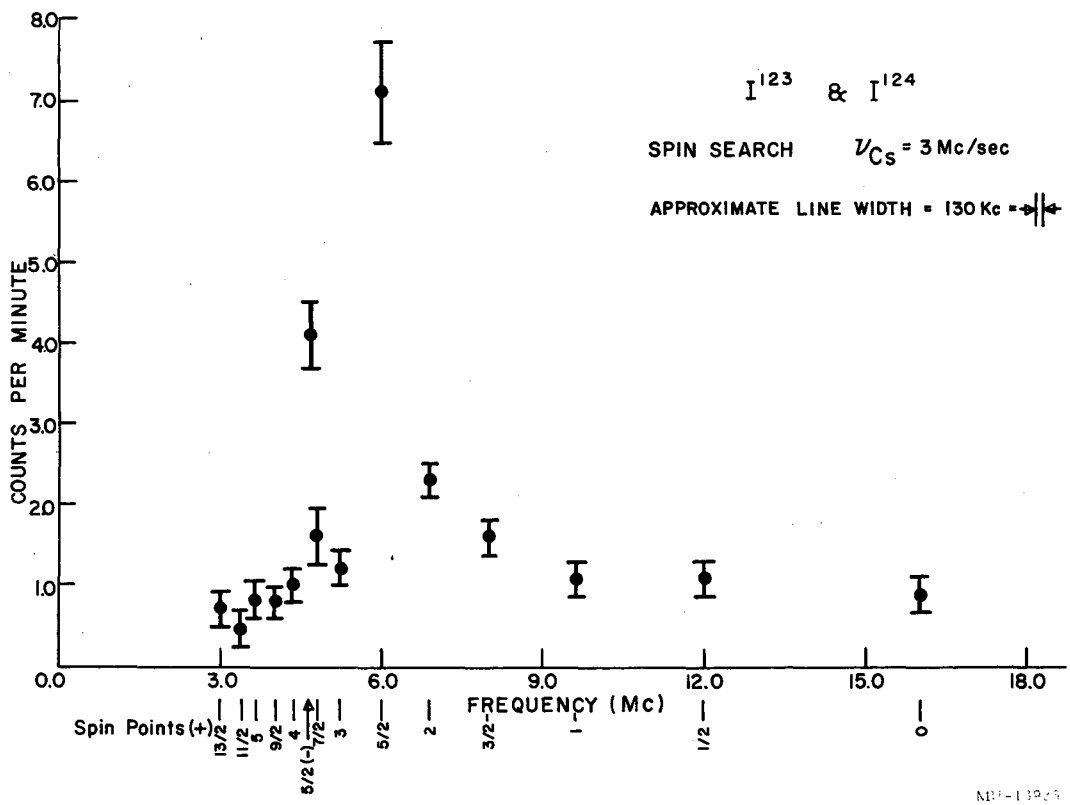

Fig. 17. Spin search on cyclotron-produced I^{123} and I^{124}. Alpha and beta resonances are indicated by + and - respectively.

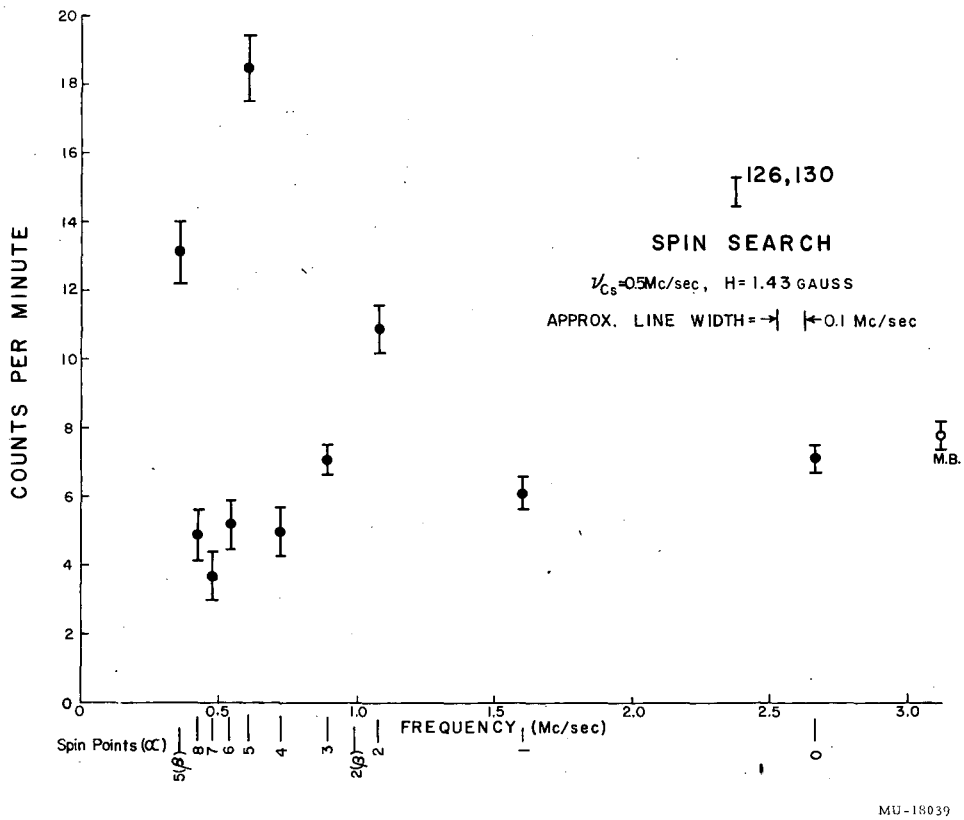

Fig. 18. Spin search on cyclotron-produced I^{126} and I^{130}.

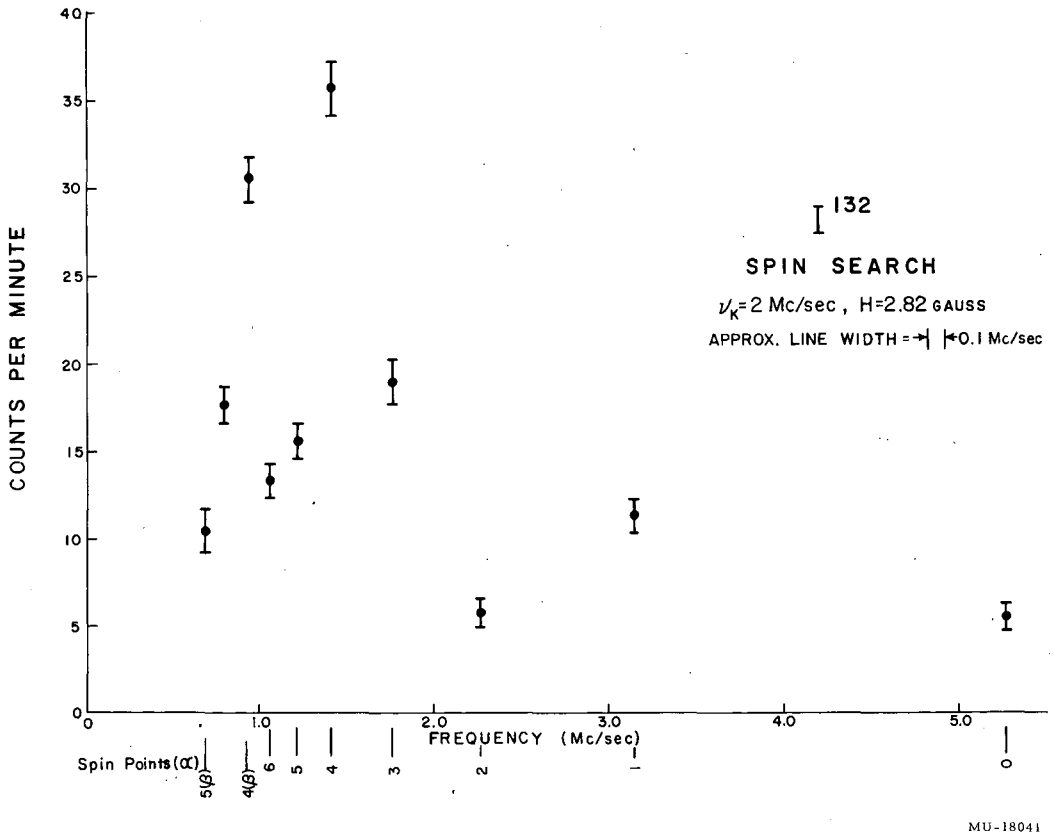

Fig. 19. Spin search on I^{132}.

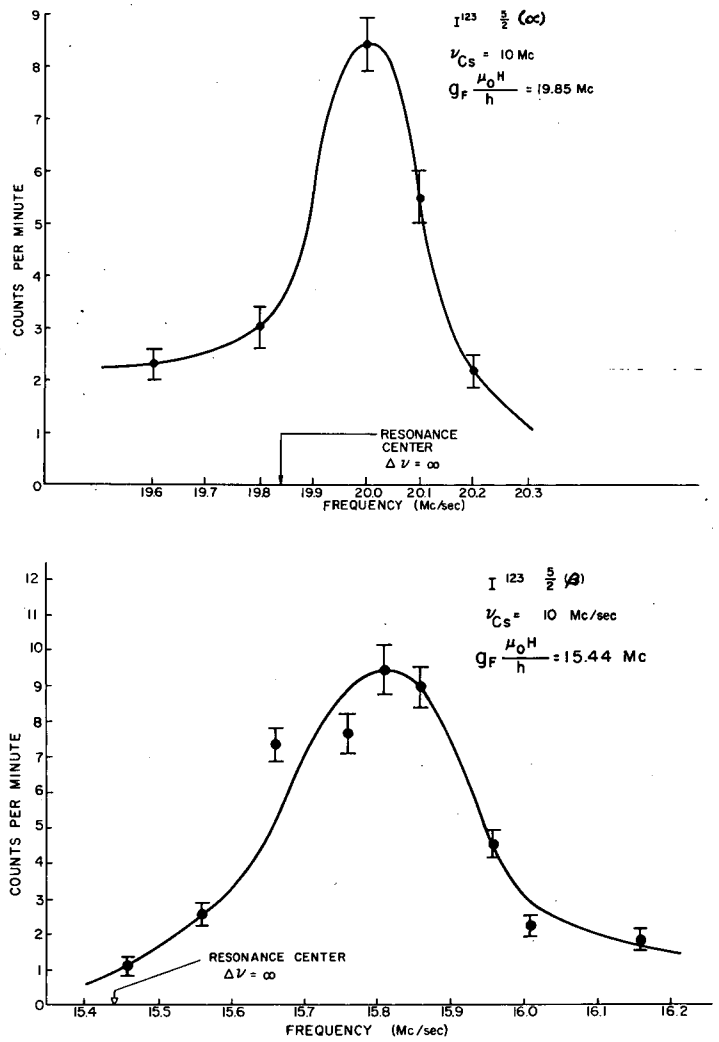

MU-18174

Fig. 20. Spin - 5/2 (α) and - 5/2 (β) resonances in I^{123}.

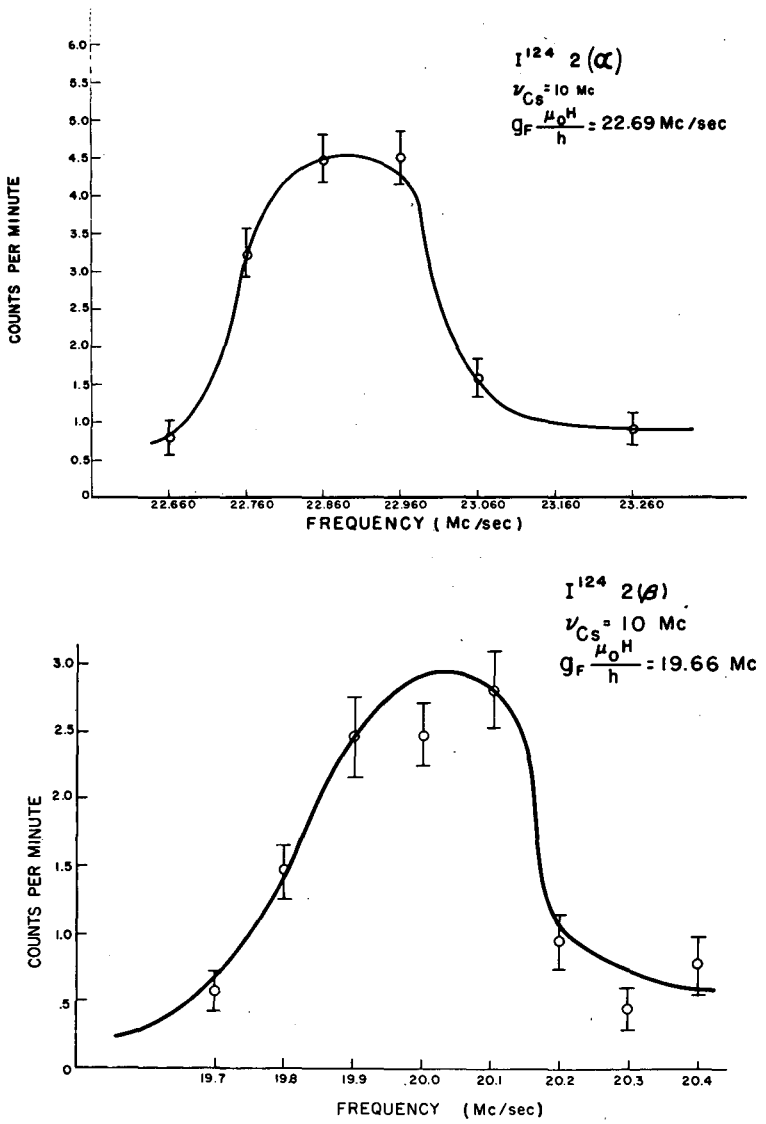

MU-18173

Fig. 21. Spin-2 (α) and -2(β) resonances in I^{124}.

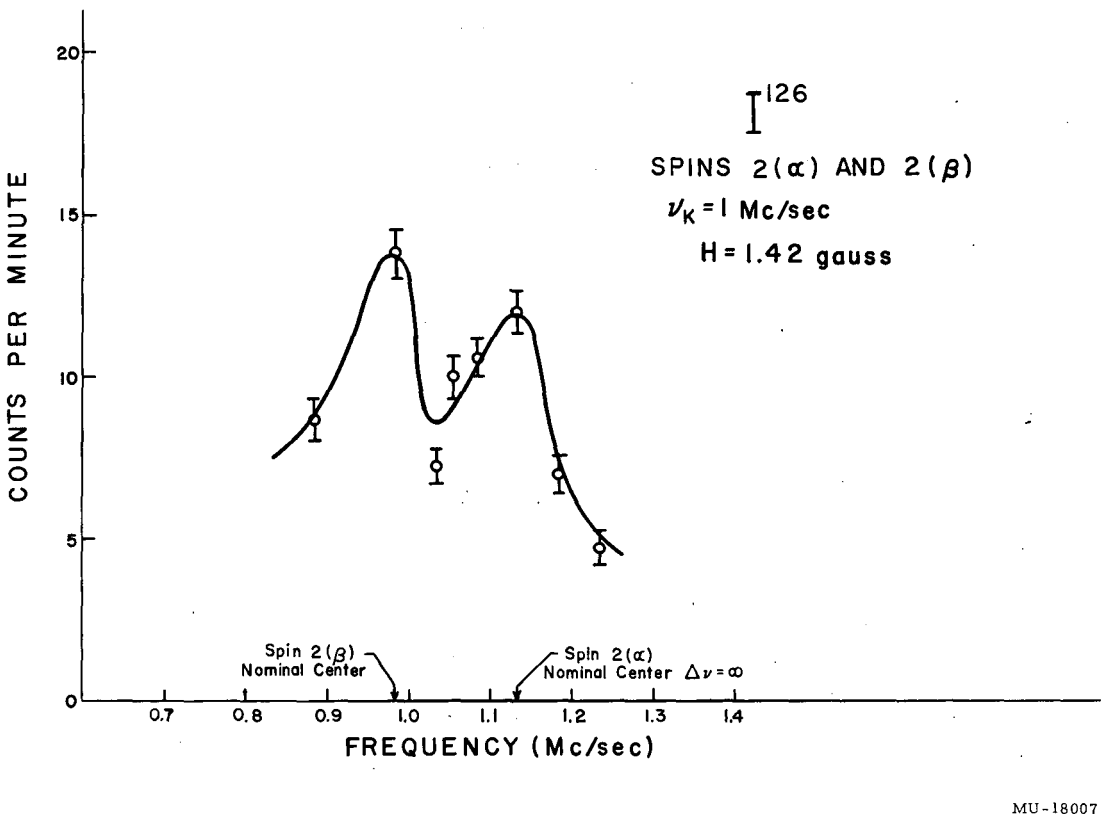

Fig. 22. Spin-2 (α) and -2 (β) resonances in I^{126}.

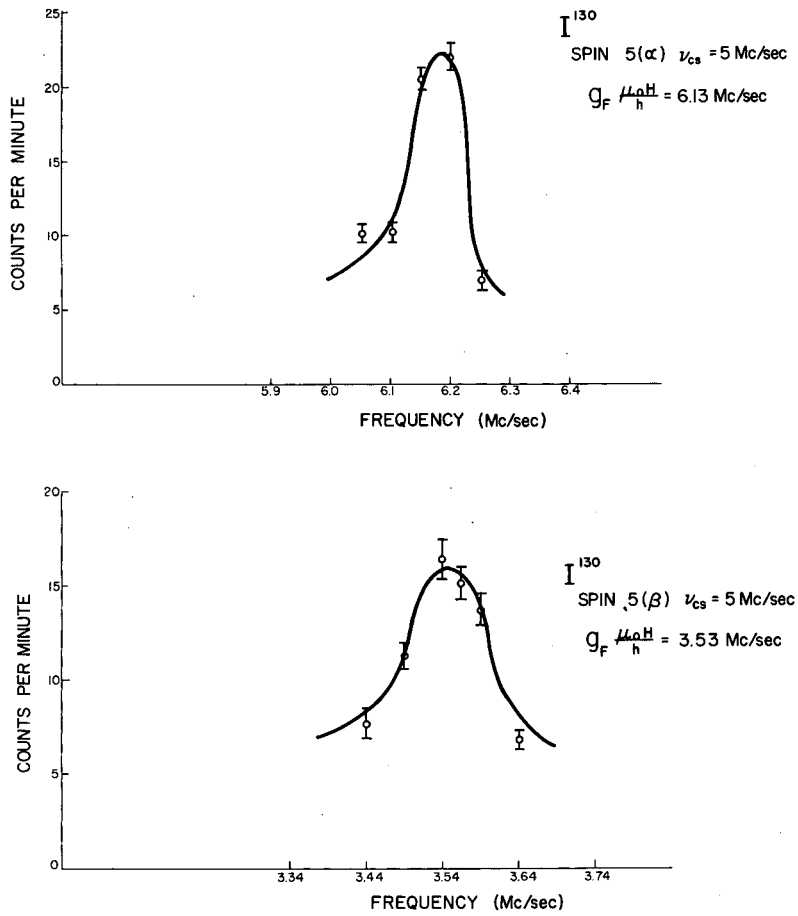

Fig. 23. Spin-5 (α) and -5 (β) resonances in I^{130}.

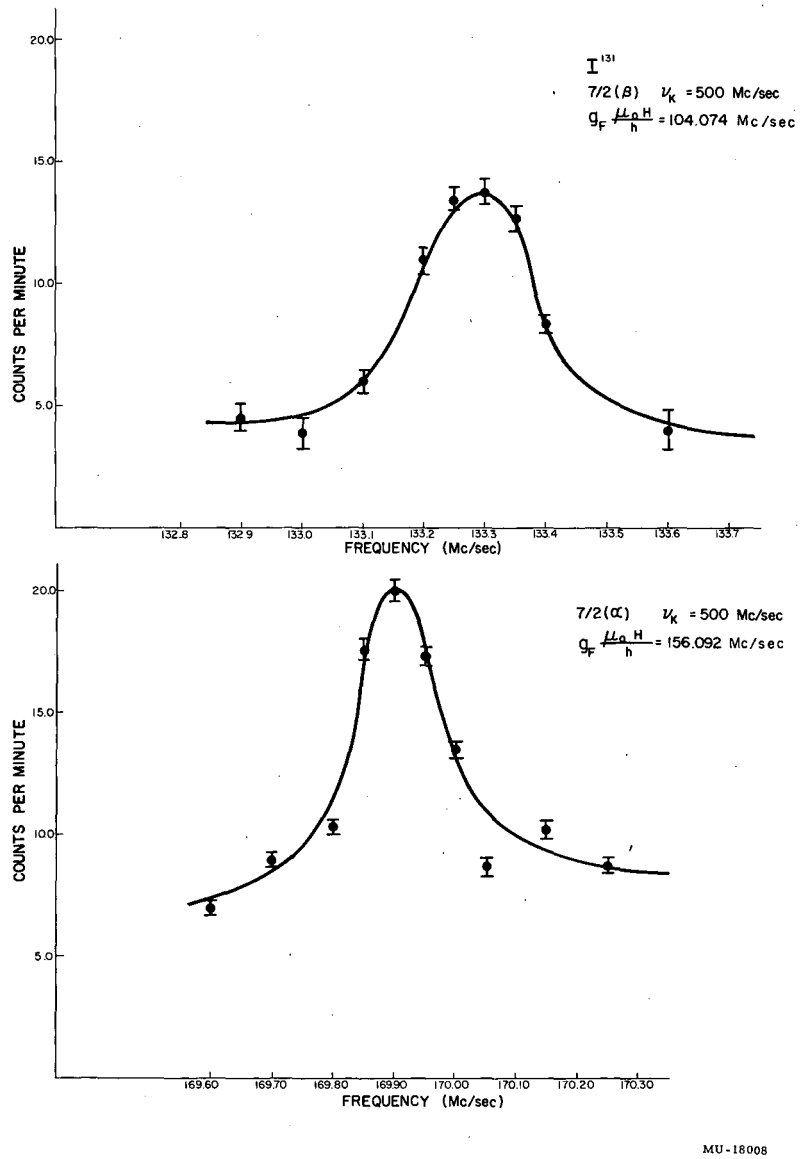

Fig. 24. Spin-7/2 (α) and -7/2 (β) resonances in I^{131}.

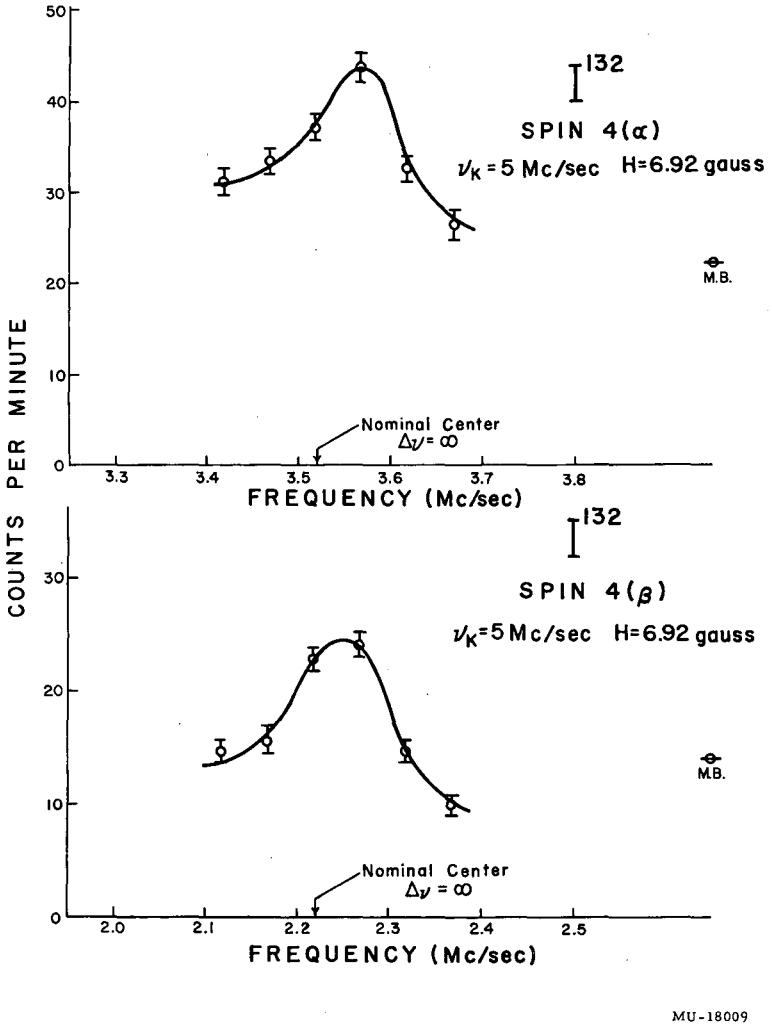

Fig. 25. Spin-4 (α) and -4 (β) resonances in I^{132}.

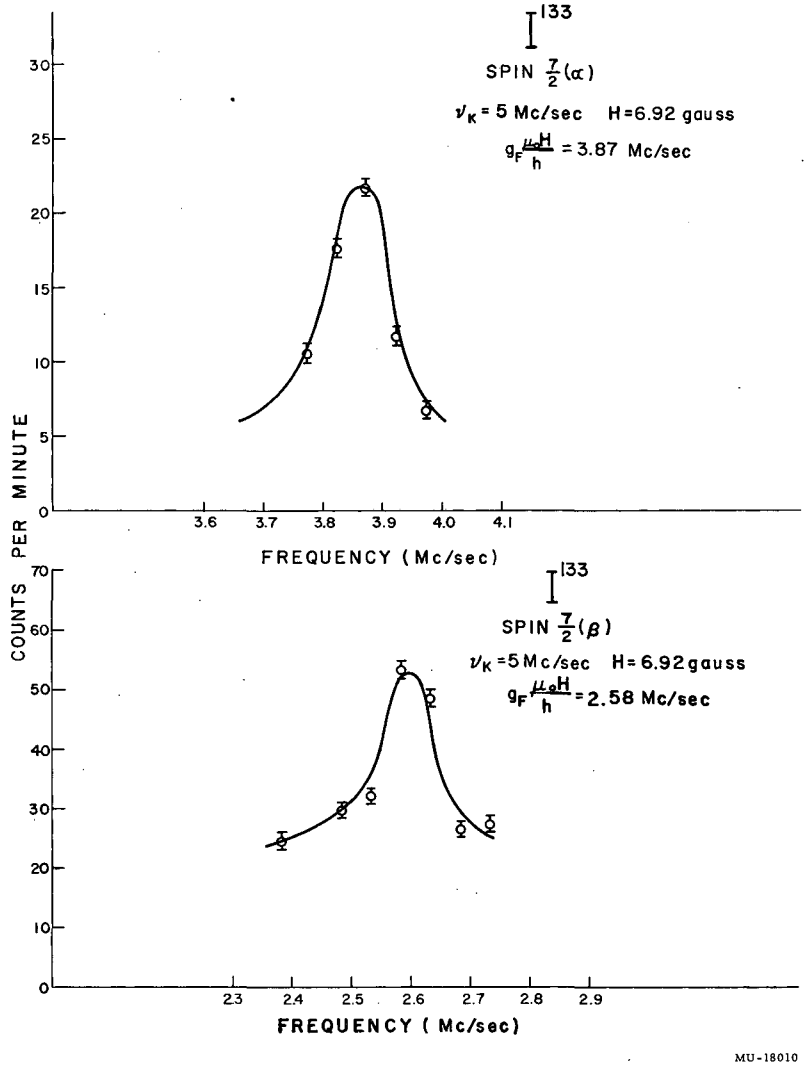

Fig. 26. Spin-7/2 (α) and -7/2 (β) resonances in I^{133}.

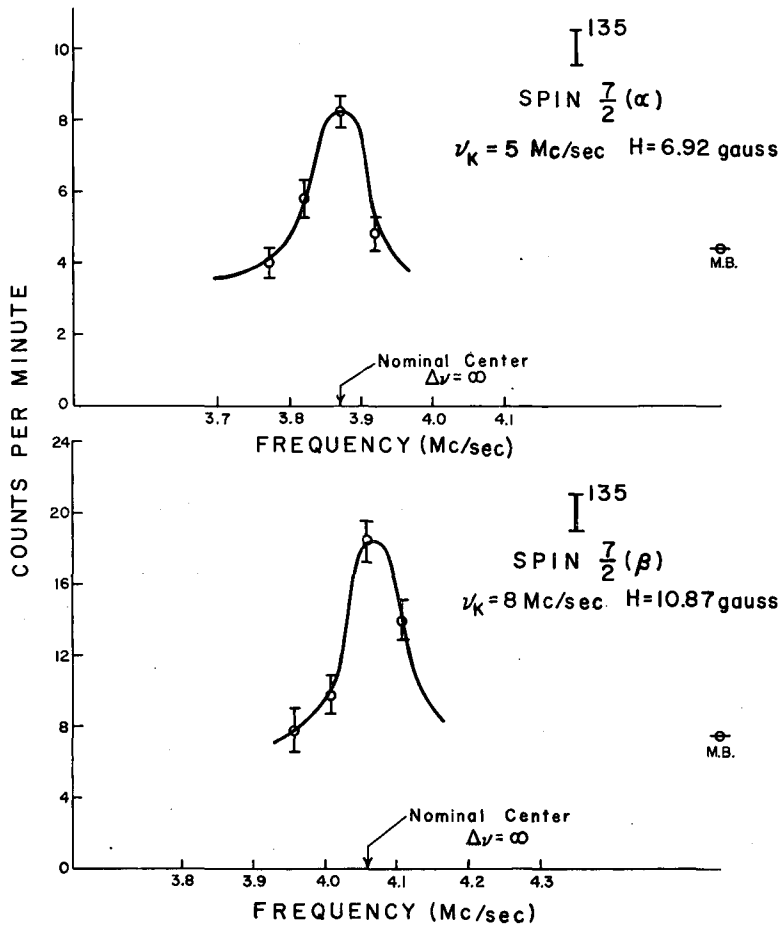

MU-18011

Fig. 27. Spin-7/2 (α) and -7/2 (β) resonances in I^{135}.

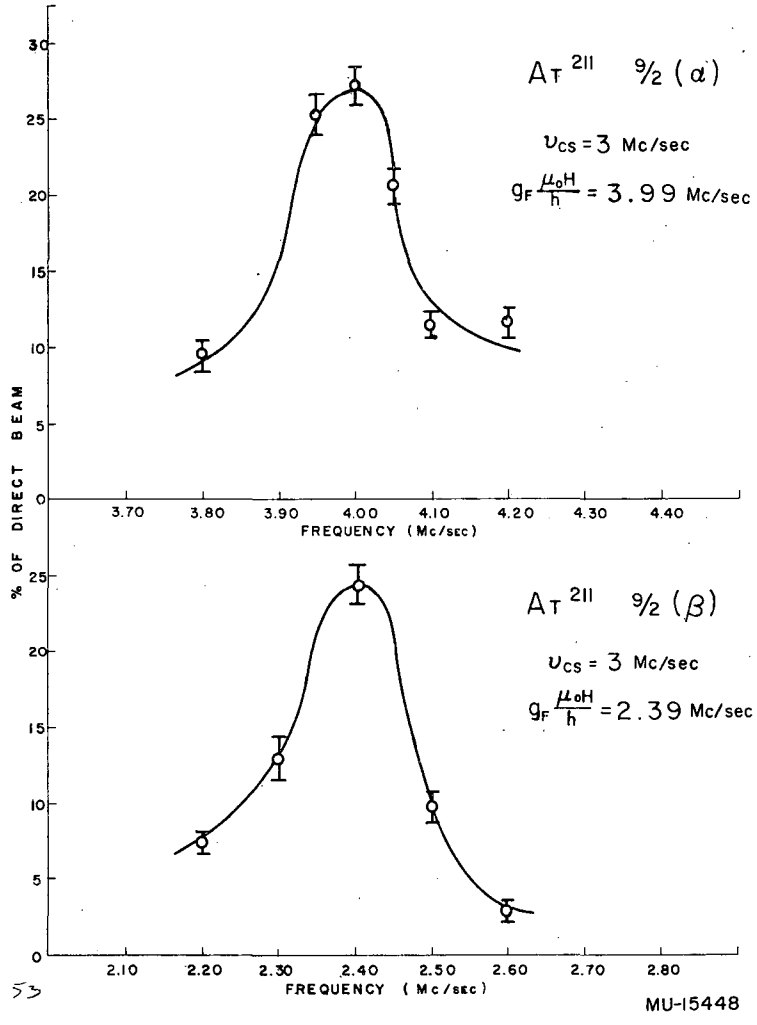

Fig. 28. Spin-9/2 (α) and -9/2 (β) resonances in At^{211}.

B. Hyperfine-Structure Measurements

According to the procedure outlined earlier for measuring hyperfine-structure constants, the hyperfine structure of I^{131} was observed directly, and the quadratic shifts in I^{132} were observed at field values high enough that approximate values of the interaction constants were obtained.

The energy-level diagram for I^{131} is given in Fig. 2. Table III summarizes the resonances observed. Note that for zero magnetic C field, the application of an rf oscillating field at a frequency equal to the hyperfine separation, $\Delta\nu_{23}$, can induce eleven different pi ($\Delta m_F = \pm 1$) resonances and also six different sigma ($\Delta m_F = 0$) resonances. As the C field deviates from zero, these resonances separate according to their field dependence in Eq. (9).

The best measurement of $\Delta\nu_{23}$ is made by observing the $(4,0) \leftrightarrow (3,0)$ transition which is field independent to first order in H_o. By Eq. (10'), however, the g_F calculated for F=3 is approximately zero, and therefore the three lines

$$(4,0) \longleftrightarrow \begin{cases} (3,1) \\ (3,0) \\ (3,-1) \end{cases}$$

remain superimposed for small values of magnetic field and tend to increase the resonance line width.

The upper direct transition $(5,-3) \leftrightarrow (4,-3)$ is a sigma

Table III

I^{131} Resonances observed			
Transition observed	Magnetic field (gauss)	Resonance frequency(Mc/sec)	Line width(Mc/sec)
$(5, -3) \overset{\alpha}{\longleftrightarrow} (5, -4)$	86.25	49.6	0.22
	278.80	169.9	0.17
	739.90	517.0	1.25
	540.17	355.75	0.75
	1049.21	805.80	1.44
$(4, -2) \overset{\beta}{\longleftrightarrow} (4, -3)$	86.25	34.90	0.19
	115.95	48.18	0.14
	278.80	133.30	0.24
	739.90	529.40	0.61
	540.17	320.95	0.69
Direct transitions:			
$(4, 0) \longleftrightarrow (3, 0)$	0.71	2138.23	0.09
$(4, 0) \longleftrightarrow (3, 0)$	4.20	2138.22	0.09
$(4, 3) \longleftrightarrow (3, 2)$	28.37	2170.09	0.18
$(4, 3) \longleftrightarrow (3, 3)$	28.37	2170.88	0.21
$(5, -3) \longleftrightarrow (4, -3)$	6.92	3289.09	0.13
$(5, -3) \longleftrightarrow (4, -3)$	2.82	3291.44	0.10
$(4, 0) \longleftrightarrow (3, 0)$	2.82	2138.21	0.09

transition that was observed at the field values indicated in Table III.

The results of the direct-transition measurements show

$$\Delta\nu_{12} = 3293.03 \pm 0.13 \text{ Mc/sec}$$

and

$$\Delta\nu_{23} = 2138.22 \pm 0.09 \text{ Mc/sec.}$$

The uncertainties quoted are the full line width of the observed resonances (at half-maximum). Estimates of effect due to configuration interaction or to the presence of an octupole moment indicate that either effect would be less than the uncertainties assigned.

As described in Chapter II an IBM-653 computer has been programmed to fit the observed resonance data to an exact solution of the Hamiltonian, Eq. (8), and to yield values of a and b appropriate to this solution. Although atomic-beam measurements of the hyperfine-structure separations determine the magnitudes of the constants a and b and their relative sign, a separate measurement is required to determine the absolute sign of a, and thus the sign of the magnetic dipole moment. This measurement must involve the interaction of the dipole moment with the external field. The theoretical frequencies calculated by the IBM-653 program involve a correction for the interaction of the nuclear moment with the external field. The correction enters into the calculated frequency as an additive term and will be positive or negative depending on the sign of the nuclear dipole

moment. Thus, as described by Garvin et al.,[26] the program provides a method for testing for the sign of the moment. The data is fitted to theoretical frequencies by assuming the sign of g_I is positive and then negative. A comparison of the closeness of fit between these two separate calculations is made, and if the difference in fit is significant, the sign may be inferred.

Table IV shows the results of the computer calculations by the use of the data of Table III. It is evident that the calculated magnitudes of a and b are the same for either sign of g_I, whereas the χ^2 values indicate that the observed data lie closer to the theoretical frequencies for ($g_I > 0$) than for ($g_I < 0$). By the use of the table of χ^2 in Fisher,[30] the comparison of calculated χ^2 values indicates a probability higher than 98% that g_I is greater than zero.*

A pictorial comparison is made in Fig. 29. The differences between observed and theoretical frequencies are shown for $g_I < 0$ and $g_I > 0$. The dashed lines indicate the experimental uncertainties.

---

*For a normal distribution of observed resonance frequencies, χ^2 would have the minimum value N-2 in fitting a function with two degrees of freedom. The χ^2 values in Table IV indicate that, on the basis of statistical arguments, there is justification in reducing the measurement uncertainties to one-fifth of the width. This would further favor the fit of $g_I > 0$.

Table IV

IBM-653 Calculations from I^{131} resonance data.

Input	a (Mc/sec)	Δa	b (Mc/sec)	Δb	χ^2
α's and β's only (10 inputs $g_I > 0$)	576.039	0.40	580.04	3.04	1.02
α's and β's only (10 inputs $g_I < 0$)	577.948	0.41	589.78	3.09	13.89
Direct trans. only (7 inputs $g_I > 0$)	575.906	0.002	578.849	0.024	4.93
All data (17 inputs $g_I > 0$)	575.906	0.002	578.849	0.024	6.03
All data (17 inputs $g_I < 0$)	575.906	0.002	578.846	0.024	33.5

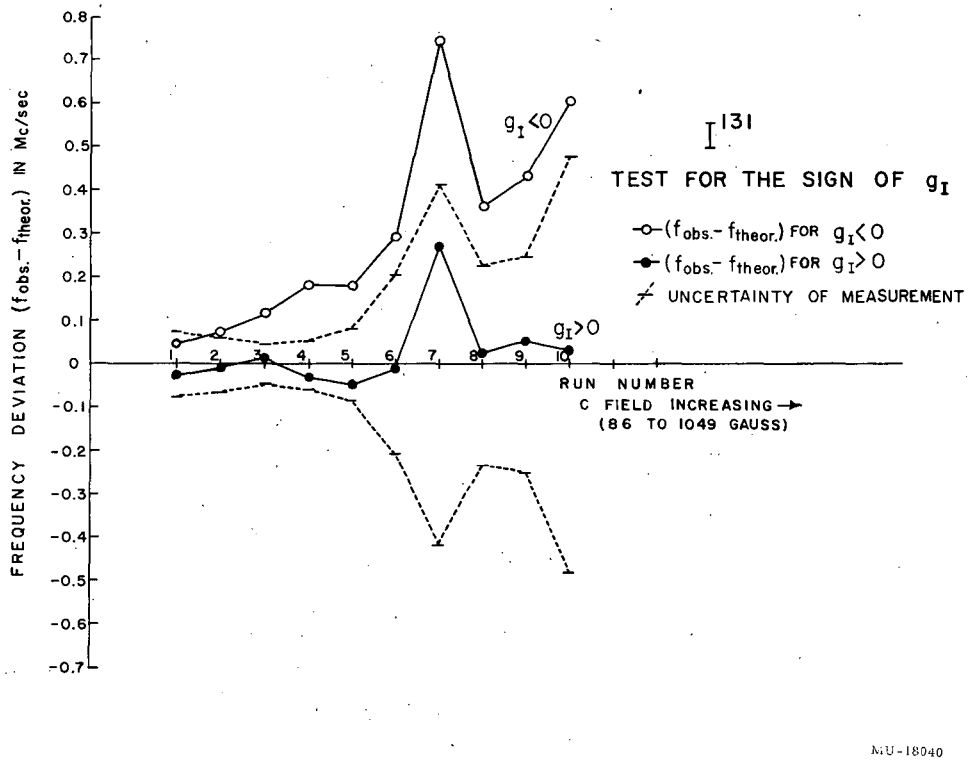

Fig. 29. Resonance frequency deviation from calculated value at best-fit conditions assuming $g_I < 0$ and $g_I > 0$.

Using the precise measurement of the magnetic dipole moment for I^{127}, $\mu_{127} = 2.8090 \pm 0.0004$ nm, by Walchi[31] and of a_{127} and b_{127} for I^{127} by Jaccarino and King,[16] we have from Eq. (15)

$$\mu_{131} = \frac{a_{131}}{a_{127}} \cdot \frac{I_{131}}{I_{127}} \cdot \mu_{127}$$

$$= 2.738 \pm 0.001 \text{ nm.}$$

Using Eq. (16), we obtain $Q_{131} = -0.412 \pm .020 \times 10^{-24}$ cm^2.

Table V shows the results of α and β transitions in I^{132}. To within the accuracy that these measurements permit, we have

$$|a| = 566 \pm 5 \text{ Mc/sec}$$

and

$$|b| = 67 \pm 36 \text{ Mc/sec.}$$

Therefore we obtain

$$\mu_{132} = \pm 3.08 \pm 0.03 \text{ nm}$$

and

$$Q_{132} = \pm 0.048 \pm 0.025 \times 10^{-24} \text{ cm}^2.$$

The supply of I^{132} was expended before the direct transitions were observed. However, the direct transitions of I^{132} will be observed in future experiments.

Table V

I^{132} Resonances observed			
Transition observed	Magnetic field (gauss)	Resonance frequency (Mc/sec)	Line width(Mc/sec)
$(11/2, -7/2) \overset{\alpha}{\leftrightarrow} (11/2, -9/2)$	6.92	3.57	0.14
	13.42	6.88	0.10
	25.39	13.02	0.08
	46.08	23.84	0.10
	89.69	47.07	0.31
	173.74	93.80	0.32
$(9/2, -5/2) \overset{\beta}{\leftrightarrow} (9/2, -7/2)$	6.92	2.25	0.12
	13.42	4.35	0.09
	25.39	8.29	0.15
	46.08	15.32	0.25
	89.69	30.80	0.25
	173.74	63.85	0.32

VI. DISCUSSION OF RESULTS

A. Nuclear-Spin Results

The isotopes of iodine and astatine considered here are in the mass range where collective nuclear effects are not expected to dominate. Thus, in this range the observed spin values might be expected to agree with the predictions of the single-particle shell model of the nucleus.[13] This was found to be the case for the majority of the isotopes. Figure 30 shows the single-particle energy levels as they are expected to be arranged for the nucleons in this mass range.[51] In cases where the number of neutrons (N) is even, the shell model predicts that the angular momentum of the nucleus will be that of the last odd proton (the fifty-third proton for iodine and the eighty-fifth, for astatine). The $5g_{7/2}$ and $4d_{5/2}$ proton energy levels are very close, and examination of the spin values of elements near iodine indicates that the order of occupying the proton levels varies sharply with the change in neutron number. In the case of ${}_{51}Sb^{121}$ (I = 5/2 [52]) the fifty-first proton may be assigned to the $4d_{5/2}$ level when N equals 70. However, it is better assigned to the $5g_{7/2}$ level when two neutrons are added to form ${}_{51}Sb^{123}$, which is found to have spin 7/2. In iodine, the proton configuration seems to be $(5g_{7/2})^2 4d_{5/2}$ for N equal to 75 or less, whereas it is $(5g_{7/2})^3$ for N between 76 and 82. Similarly for cesium the spin change from 5/2 to

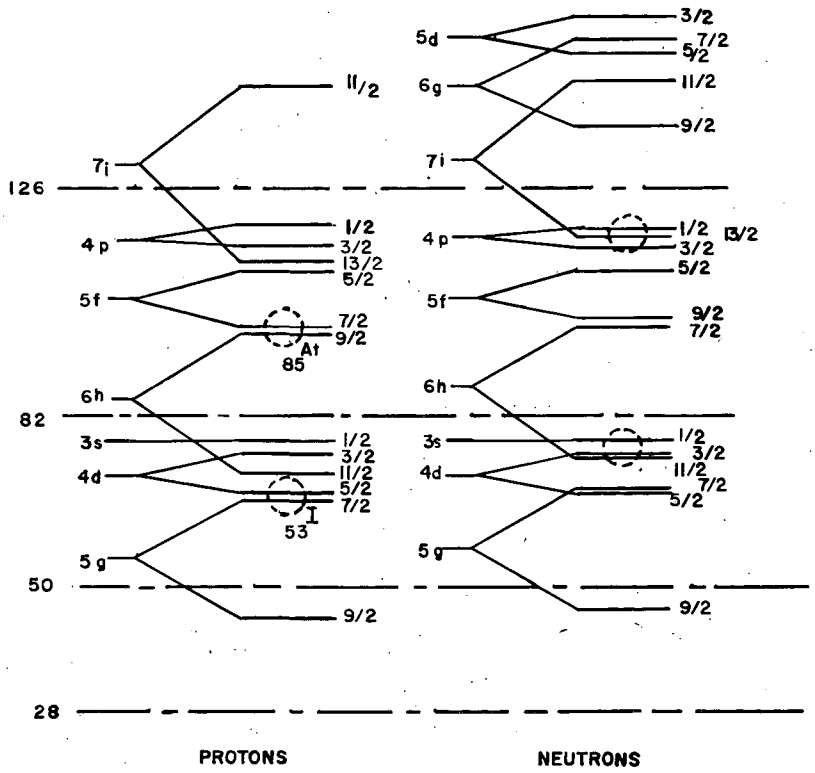

MU-18013

Fig. 30. Single-particle shell-model nuclear energy levels for Z or N greater than 50. Proton and neutron levels for iodine and astatine are in the regions indicated (see Ref. 51).

7/2 takes place for N equals 77.

Table VI illustrates the consistent manner in which the odd-proton--even-neutron configuration in iodine may be related to the observed spin values. The level assignments assumed in Table VI are consistent with the observed spins and moment values of odd-proton--even-neutron isotopes or of even-proton--odd-neutron isotopes in the elements adjacent to iodine. Although the neutron level is close to the $3s_{1/2}$ and $4d_{3/2}$ levels, the observed spin values (e.g., for Xe^{129}, Xe^{131}, Te^{123}, and Te^{125}) indicate that an odd neutron tends to occupy the lower angular-momentum levels, whereas the $6h_{11/2}$ level is filled only by pairs of neutrons.

For cases where N is also odd, the total nuclear spin must result from a coupling of the odd-neutron and odd-proton configurations. Although the manner of such coupling is not completely understood,[53] experimental evidence supports Nordheim's rules in regions near the filled shells.[54] These rules result from the tendency of a single proton and single neutron to couple together in such a manner that their intrinsic spins are aligned parallel. Two rules result for this coupling:

(a) Strong rule: If one of the odd nucleons is in a level with intrinsic spin and orbital angular momentum parallel and the other in a level where they are antiparallel, then the total angular momentum of the ground state is the smallest

Table VI

Iodine spins by the single-particle shell model															
Proton assignment	Neutron assignment	Nordheim prediction	I^{123}	I^{124}	I^{125}	I^{126}	I^{127}	I^{128}	I^{129}	I^{130}	I^{131}	I^{132}	I^{133}	I^{134}	I^{135}
$(5g_{7/2})^2(4d_{5/2})$	even	$I = 5/2$	5/2		5/2		5/2								
$(5g_{7/2})^3$	even	$I = 7/2$							7/2		7/2		7/2		7/2
$(5g_{7/2})^2(4d_{5/2})$	$(3s_{1/2})$	$2 < I \leq 3_{weak}$		2		2									
	$(4d_{3/2})$	$I = 1_{strong}$						1							
$(5g_{7/2})^3$	$(3s_{1/2})$	$I = 3_{strong}$													
	$(4d_{3/2})$	$2 < I \leq 5_{weak}$								5		4		( )	

possible, i.e., for

$$j_n = l_n \pm 1/2 \text{ and } j_p = l_p \mp 1/2 \text{ we have } I = \left| j_n - j_p \right| ,$$

where the l's and j's are the orbital and total angular momentum of the neutron (n) or proton (p) levels.

(2) Weak rule: If both the proton and neutron are in levels in which intrinsic spin and orbital angular momentum are parallel or if both are in levels in which spin and orbital angular momentum are antiparallel, then the angular momenta, j_n and j_p tend to add, although not necessarily to the highest possible value. That is, for

$$j_p = l_p \pm 1/2 \text{ and } j_n = l_n \pm 1/2, \text{ we have } I = j_p + j_n.$$

As discussed by Way et. al.,[55] this rule may be written

$$\left| j_p - j_n \right| < I \leqslant (j_p + j_n). \tag{17}$$

Again from Table VI it may be seen that the majority of the observed spin values of the odd-odd nuclei of iodine fit the prediction of Nordheim's rules.

Nordheim's weak rule, as it is written in Eq. (17), admits the possibility of a wide range of values for the resultant spin. Recent studies by Schwartz[56] indicate that in nuclei that have one type of nucleon (e.g., protons) outside of a closed shell, but the other type (i.e., neutrons) missing from a shell, the resultant ground-state angular momentum may be given as

$$I = (j_p + j_n - 1). \tag{18}$$

The level assignments for I^{124} and I^{126} in Table VI are inconsistent with Nordheim's rule as given in Eq. (17) but do satisfy Eq. (18).

The level assignment of I^{126} is inconsistent with the assignment of the ($5g_{7/2}$, $6h_{11/2}$) odd-proton--odd-neutron configuration as based upon β and γ -ray studies.[57, 58]

The nuclear spin of I^{128} was measured in an atomic-beam experiment by J. E. Sherwood at the Oak Ridge National Laboratory.[59] The value was found to be 1, which is consistent with the spectroscopic measurements by Benczer et. al.,[60] and also consistent with the ($4d_{5/2}$, $4d_{3/2}$) configuration assignment.

The measured value of spin 5 for I^{130} is in agreement with the atomic-beam measurement made simultaneously by Sherwood,[61] but in disagreement with the nuclear-spectroscopic results of Caird and Mitchell,[62] who made the assignment of 6 (-) on the basis of the log (ft) values of the 1.02-Mev decay to Xe^{130}.

The β decay scheme of I^{132} to Xe^{132} was studied by Finston and Bernstein, but no spin assignment was made.[63] The spin value of 4 for this isotope might be considered to represent coupling to ($j_n + j_p - 1$) as in Eq. (18). The spin of 5 for I^{130} (with five neutrons missing from the filled shell) requires the maximum coupling to ($j_p + j_n$). In such case the spin-spin and spin-orbit interactions must dominate over the orbit-orbit interactions of the odd nucleons.

Astatine-211 contains a magic number of neutrons (N = 126) and the proton shells are filled at $Z = 82$. The observed spin of 9/2 is simply understood on the basis of the single-particle shell model by assigning the three protons to the $6h_{9/2}$ level. Two of the protons pair, and the spin is determined by the last odd proton.

B. Hyperfine-Structure Results

The hyperfine-structure measurements of I^{131} were intended to verify and improve the previously published values of $\mu_{131} = 2.56 \pm .12$ by Fletcher[64] and $I = 7/2$, $Q_{131} = 0.412 \times 10^{-24}$ cm^2 by Livingston et al.[65] Fletcher's results for μ_{131} are based upon the comparison of g factors between I^{131} and I^{127}. Although he uses the same value of μ_{127} as used in the results reported in Chapter IV,[31] his results differ from the atomic-beam value by more than the sum of the experimental uncertainties. As mentioned in Chapter II, the octupole interaction term and the effect of configuration interaction are neglected in these atomic-beam results. If the effects of these interactions are assumed to be of the order of those observed by Jaccarino in I^{127},[16] the experimental results are still in disagreement with Fletcher's.

On the basis of a pure single-particle shell model, the value of μ_{131} (Schmidt value) would be expected to be $\mu_{g_{7/2}} = 1.718$ nm. Thus the magnetic dipole moment of I^{131}

deviates even farther from the Schmidt lines than does that for I^{129} (μ_{129} = 2.6173 ± 0003 nm.[31])

The measured value of $Q_{131} = -0.412 \times 10^{-24}$ cm^2 is in agreement with the published value by Livingston et al.[65] obtained by microwave absorption experiments in which the quadrupole interaction constant (eqQ) for I^{131} was compared with that for I^{127}. The value of Q_{131} was then calculated from the value of Q_{127} based upon Jaccarino's atomic-beam measurements.

Although the single-particle level assignments have been found to give good agreement with measured nuclear spin values, the observed magnetic dipole moments and electric quadrupole moments differ widely from those values expected for a single particle. These deviations may be attributed to the asymmetry of the nuclear core. Two empirical rules have been proposed to correlate the variation in magnetic moments and core asymmetry (which is related to the quadrupole moment):

(a) Bohr proposes that, of two isotopes with the same spin and differing only by two neutrons, the nucleus with the numerically smallest quadrupole moment has a magnetic moment closest to the pure-state value (Schmidt value).[9]

(b) Gordy, on the other hand, proposes that the magnetic moment decreases as the nucleus becomes more elongated (i.e., Q increases for positive Q values or decreases numerically for negative Q values).[66] Applying these rules to the comparison of I^{129} and I^{131}, we have

$$\mu_{129} = 2.617 \text{ nm} < \mu_{131} = 2.738 \text{ nm},$$

and

$$Q_{129} = -0.574 \times 10^{-24} \text{ cm}^2 < Q_{131} = -0.412 \times 10^{-24} \text{ cm}^2.$$

It is apparent that neither rule is consistent with the observed properties.

The value of Q can be calculated [from Eq. (6)] by an alternative procedure which uses the fine-structure separation, δ_{FS}, to obtain a value of $\langle r^{-3} \rangle$; δ_{FS} is related to $\langle r^{-3} \rangle$ by the expression[22]

$$\delta_{FS} = \frac{\mu_0^2}{hc} Z_i^* (2L + 1) \mathcal{H} \langle r^{-3} \rangle . \tag{19}$$

Here δ_{FS} is 7603 cm^{-1}, Z_i^* is the effective value of the nuclear charge, and $\mathcal{H}$ is a relativistic correction factor tabulated by Kopfermann.[20] Barnes and Smith have shown that Z_i^* approximately equals $Z - n$, n being the radial quantum number of the valence electron.[67] Using the value $b_{131} = 578.85$ Mc and the Sternheimer correction, $C = 1.029$, one obtains, from Eqs. (6) and (19),

$$Q_{131} = (-0.35 \pm .04) \times 10^{-24} \text{ cm}^2.$$

This value is slightly less than the value obtained by the elimination of $\langle r^{-3} \rangle$ and the use of Eq. (16). Murakawa has performed a similar calculation for I^{127};[68] using Jaccarino's value of b_{127} and assuming $Z_i^* = 53 - 4 = 49$, he arrives at a value of $Q_{127} = (-0.69 \pm .03) \times 10^{-24} \text{ cm}^2$. Murakawa explains that this value is different from that obtained by eliminating

$\langle r^{-3} \rangle$ and using the value of a_{127} because the ground state is not a pure $^2P_{3/2}$ state but instead is a mixture due to the presence of the $5s5p^5 6s$ configuration. This mixture has the effect of diminishing $a_{127}(^2P_{3/2})$ in the manner illustrated by Koster.[69] An atomic-beam measurement of a_{127} in the $^2P_{1/2}$ state (as was done in chlorine by Davis et al.[14]) would be of use in determining the extent to which mixing occurs. Optical measurements have been made of the hyperfine splitting in the $^2P_{1/2}$ state, but the results to date are not precise enough to measure the effect of mixing.[70] Although the values of μ_{132} and Q_{132} for I^{132} are quite inexact (as they represent only preliminary values), they do show two interesting features: (a) The high value of $\mu_{132} = \pm 3.08$ nm is not far removed from the pure-state value ($\mu = 2.87$ nm) that would be obtained if the moments of the $5g_{7/2}$ proton and $4d_{3/2}$ neutron configurations were assumed to add; (b) the very small value of $Q = \pm 0.048 \times 10^{-24}$ cm^2 indicates that the addition of one neutron to the nucleus of I^{131} has caused a nine-fold reduction in the effective quadrupole moment. A more exact comparison, using the collective model of the nucleus,[10] would be in terms of the deformation parameters, δ, of the nuclear core in each of the two isotopes. The measured value of Q is related to δ (as shown by Nilsson[12]) by

$$Q = 0.8\, Z\, (R_Z)^2\ \delta\ (1+2\delta/3)\ \frac{I(2I-1)}{(I+1)(2I+3)}\ , \qquad (20)$$

where R_Z is taken equal to the radius of charge of the nucleus or

R_Z = 1.2 times $10^{-13}A^{1/3}$ cm. From Eq. (20) the deformation, δ of I^{132} is approximately one tenth that of I^{131}.

ACKNOWLEDGMENTS

The completion of this research project has been made possible by the support of many to whom I am indebted. I owe my deepest thanks:

To Professor William A. Nierenberg, my research director, for his kind support, able guidance, and inspirational zeal.

To Dr. Edgar Lipworth for sharing with me his knowledge of theoretical concepts and experimental techniques.

To Drs. Howard A. Schugart, John C. Hubbs, Kenneth M. Smith and the other members of the atomic-beam group who have contributed many helpful suggestions and advice.

To Drs. James C. Wallmann and Earl K. Hyde, and Messrs. Evan H. Appleman, Ralph D. McLaughlin, and John M. Alexander of the Radiation Laboratory Chemistry Department for their expert advice in the development of sample-preparation techniques.

To Messrs. Thomas M. Green, Lawrence M. Cohen, and John R. Padilla for their able assistance in the operation of the atomic-beam apparatus.

To Messrs. W. Barton Jones and Peter F. McWalters and the 60-in. cyclotron Staff who sought continually to provide the radioactive samples for this research. Also to Messrs. L. John Cooper and John E. Bowen and the Health Chemistry staff who insured conditions of safety in handling these samples.

To Messrs. Douglas B. MacDonald, Gartland G. Young, and

the accelerator technicians who skillfully designed and produced much of the mechanical equipment that comprised the atomic-beam apparatus.

And finally, to my beloved wife and family who have endured these lean years in order that I might continue my graduate education.

This work was performed under the auspices of the U. S. Atomic Energy Commission.

APPENDIX A

Identification of Isotopes

The production techniques described in Chapter III serve to specify the range of isotopes which are expected to be present in a radioactive sample. The chemical-separation techniques enhance the purity of the iodine or astatine; however, there still may be more than a single isotope present in the atomic beam. The decay half-lives of the neighboring isotopes of iodine are generally different enough that identification of spin resonances may be made by half-life analysis.

The full-beam decay of the antimony produced isotopes, Fig. 31, shows a composite decay of 13-hr I^{123} and 4.5-day I^{124}. The long tail in the decay is due to the presence of 60-day I^{125}. Figures 32 and 33 show the decay plots of resonance buttons for spin 5/2 and spin 2. In each case the decay half-life is essentially the published value.

The full-beam decay of iodine produced in the tellurium target, shows the presence of 12.6 hr I^{130}, and also 13-day I^{126}. In the spin search on this sample (Fig. 18), half-life analysis of the resonance buttons was necessary to identify the isotopes present. The activity on the spin buttons is high for spin 5 and spin 2. The decay of the spin 5 button is faster than the full beam itself and indicates that the counting is primarily

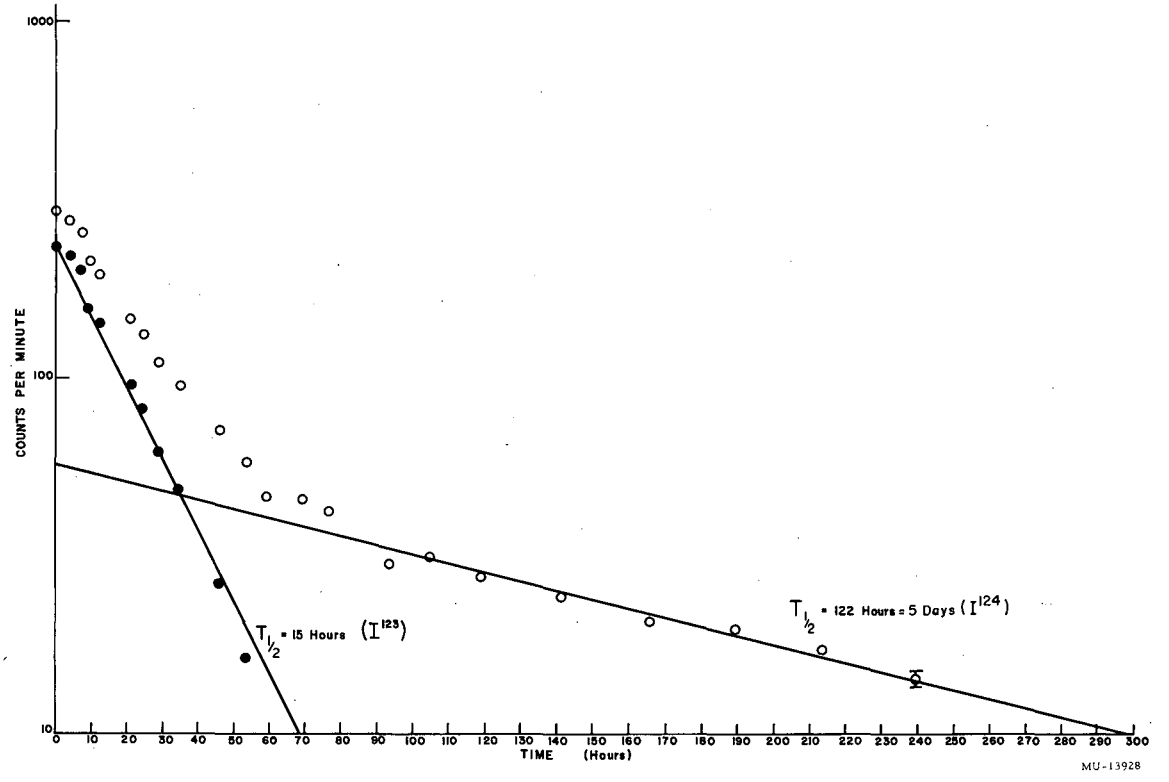

Fig. 31. Decay of full-beam button containing cyclotron-produced I^{123} and I^{124}.

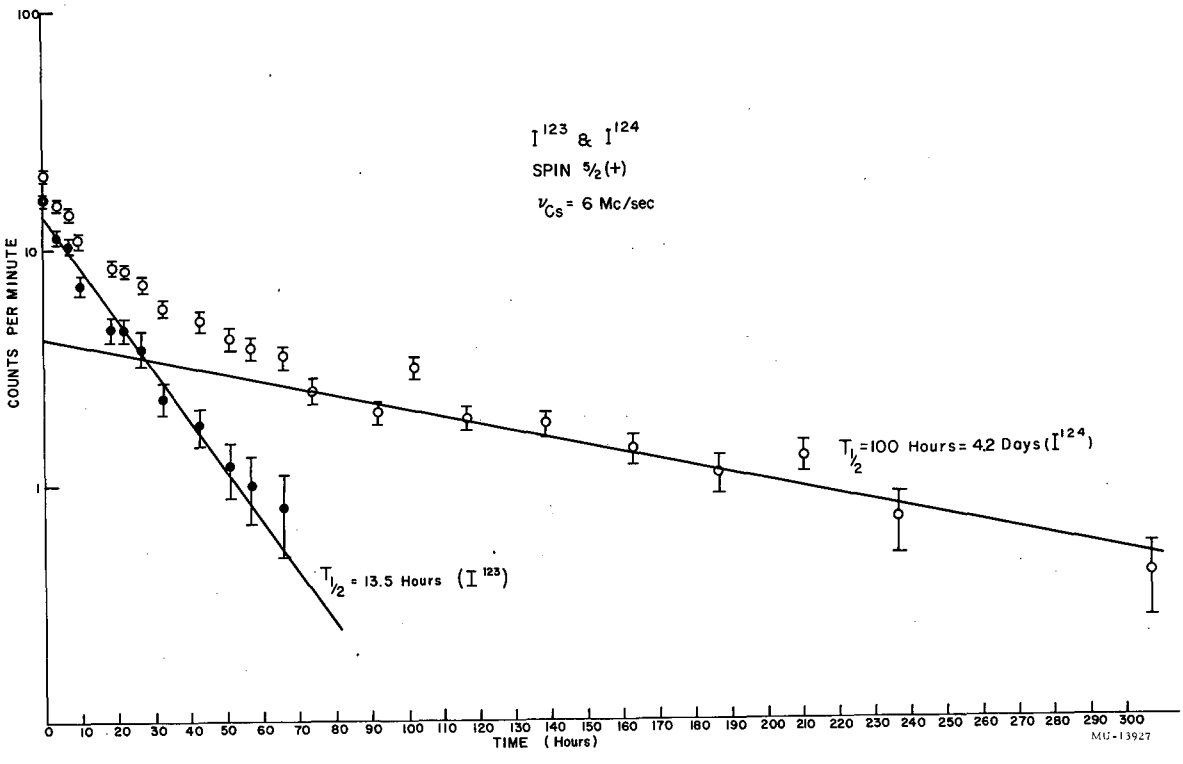

Fig. 32. Decay of spin-5/2 (α) resonance peak buttons in cyclotron-produced I^{132} and I^{124}. The short-lived component is due to I^{123} with spin 5/2; the long-lived component arises from overlap from the I^{124} 2 (β) resonance. Alpha resonances are indicated by + .

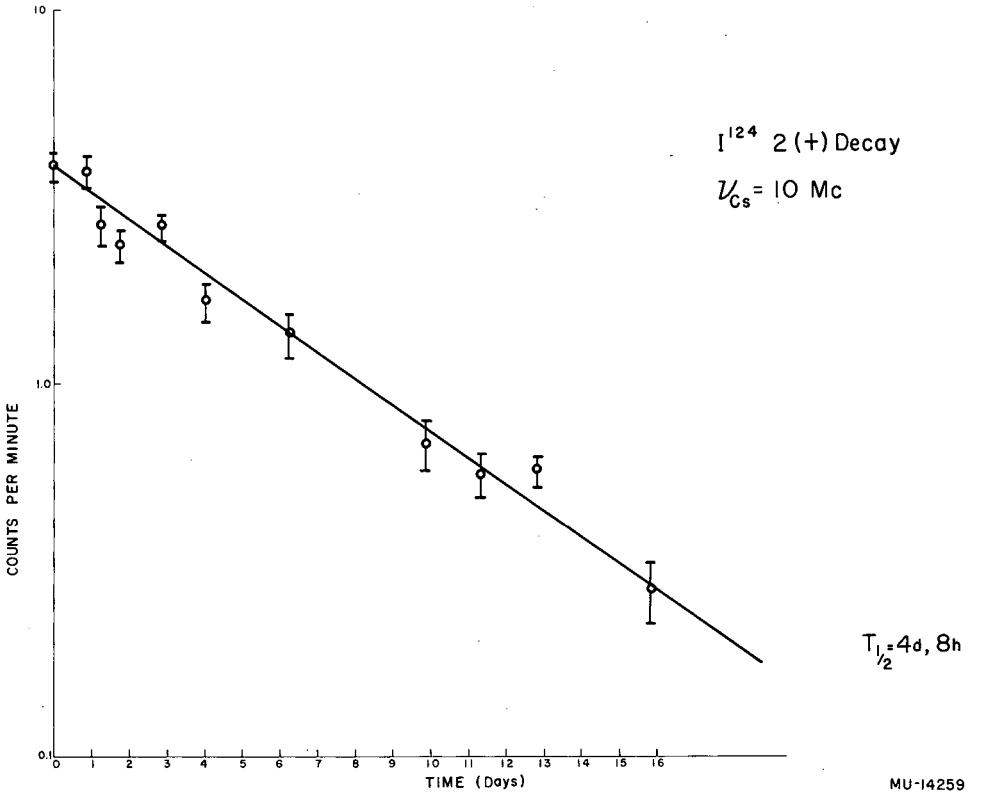

Fig. 33. Decay of spin-2 (α) resonance peak button in I^{124}. Alpha resonances are indicated by +.

due to I^{130}. The activity on the spin-2 button is found to decay very slowly, at a rate appropriate to atoms of I^{126} (see Fig. 34).

In the analysis of the iodine isotopes produced by the fission of U^{238} by deuteron bombardment, the full-beam decay (Fig. 35) is complex but consistent with that expected for a mixture of I^{132} through I^{135}. Decays of spin-resonance samples (Fig. 36) serve to identify the spin assignment of I^{135}.

The I^{133} sample obtained from Brookhaven has some I^{131} mixed with it. Therefore the full-beam button shows a composite decay. The spin values of the two isotopes are the same, and so the spin-resonance decay is also composite (see Fig. 37).

Both I^{131} and I^{132} were studied as essentially pure isotopes with the result that the decays of their full-beam and resonance buttons are quite pure and the half-lives are consistent with published values. The decays of the full-beam and spin 4(α)-resonance buttons for I^{132} are shown in Fig. 38.

In the bombardment of Bi to produce At^{211}, the bombarding energy was kept below 29 Mev in order that the sample have little or no At^{210} present. As a result, the full beam and spin buttons showed essentially the pure 7.5-h4 decay characteristic of At^{211} (see Fig. 39).

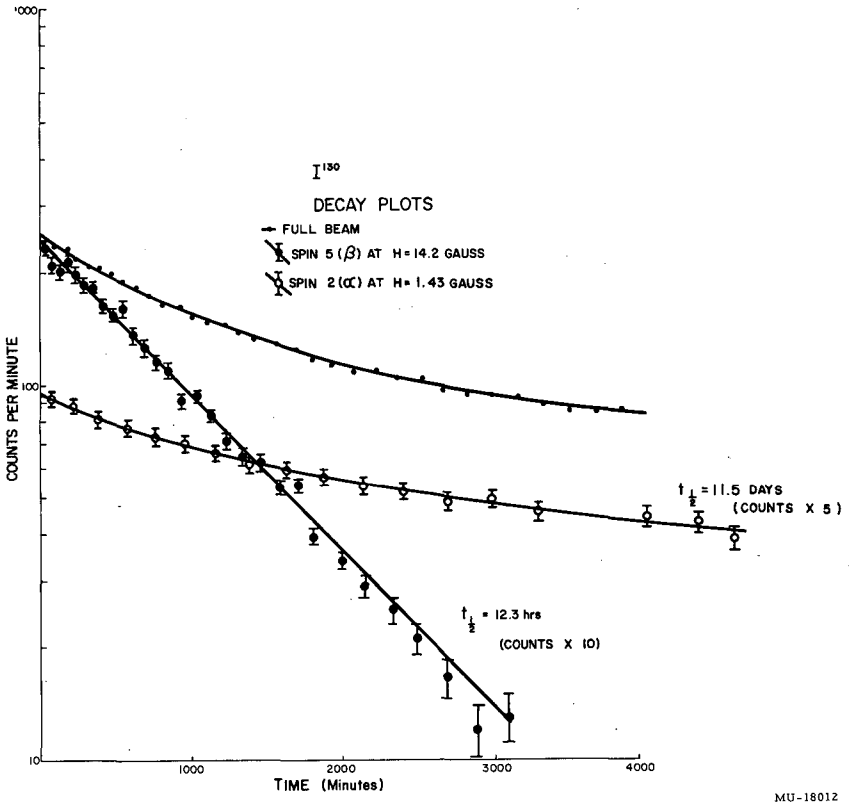

Fig. 34. Decay of full-beam button and spins-5 (α) and -2 (α) resonance-peak buttons due to I^{130} and I^{126}.

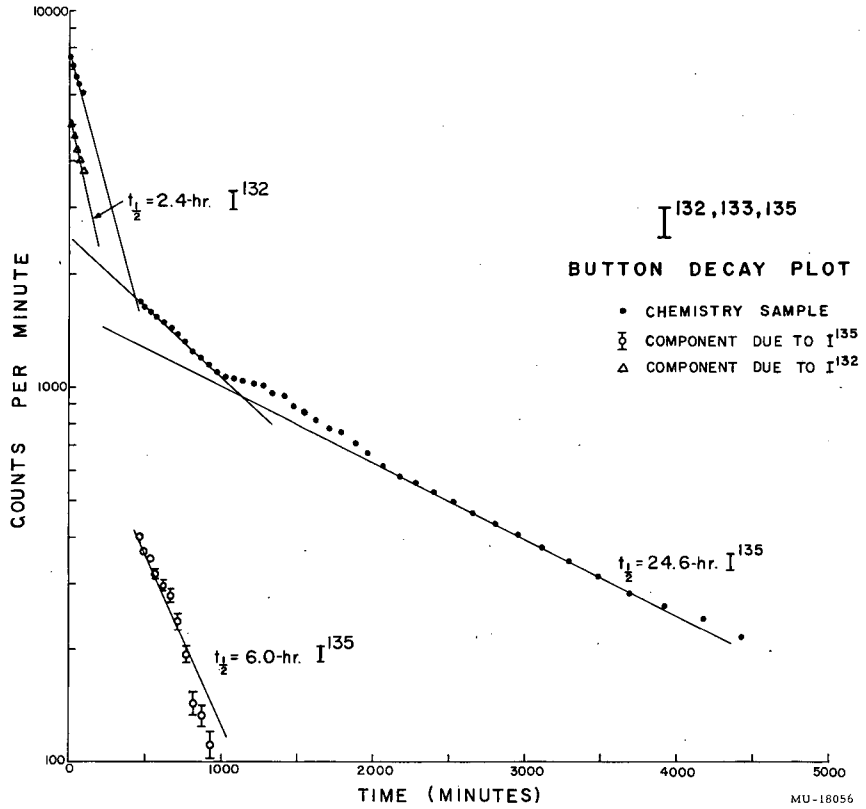

Fig. 35. Decay of chemistry-sample button containing I^{132}, I^{133}, and I^{135} produced by fission of U^{238} by deuteron bombardment.

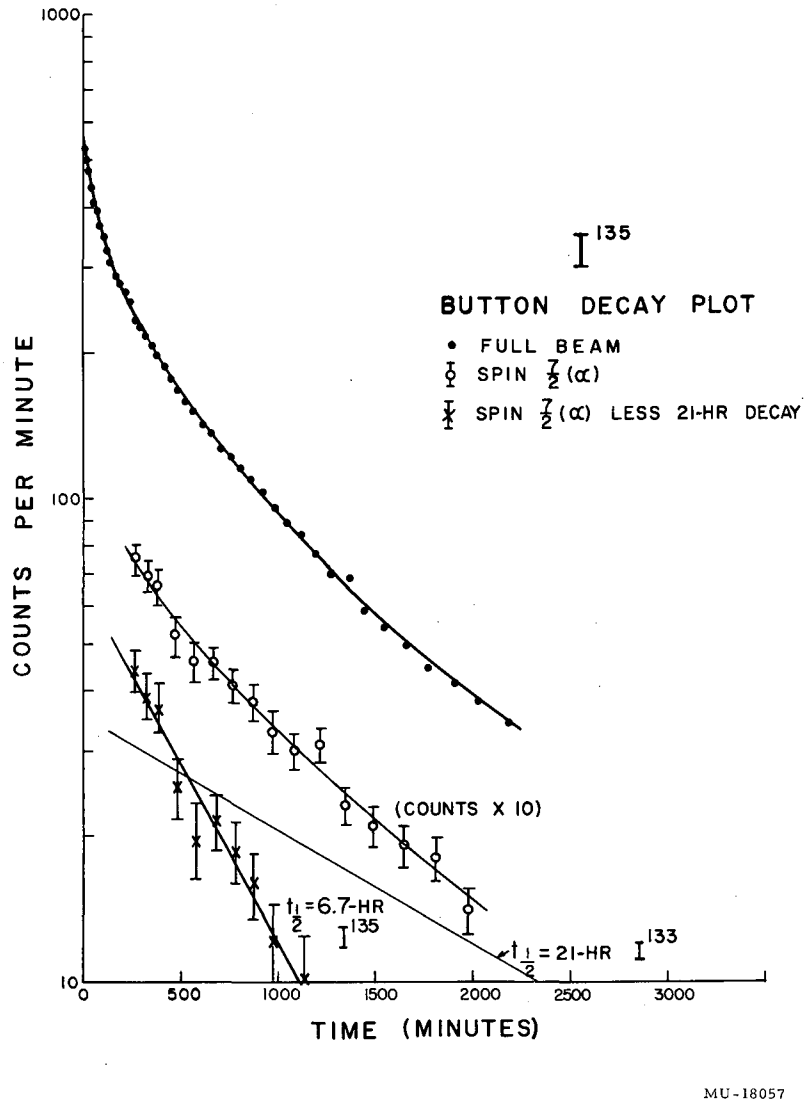

Fig. 36. Decay of full-beam and spin 7/2 (α) resonance buttons in I^{135}.

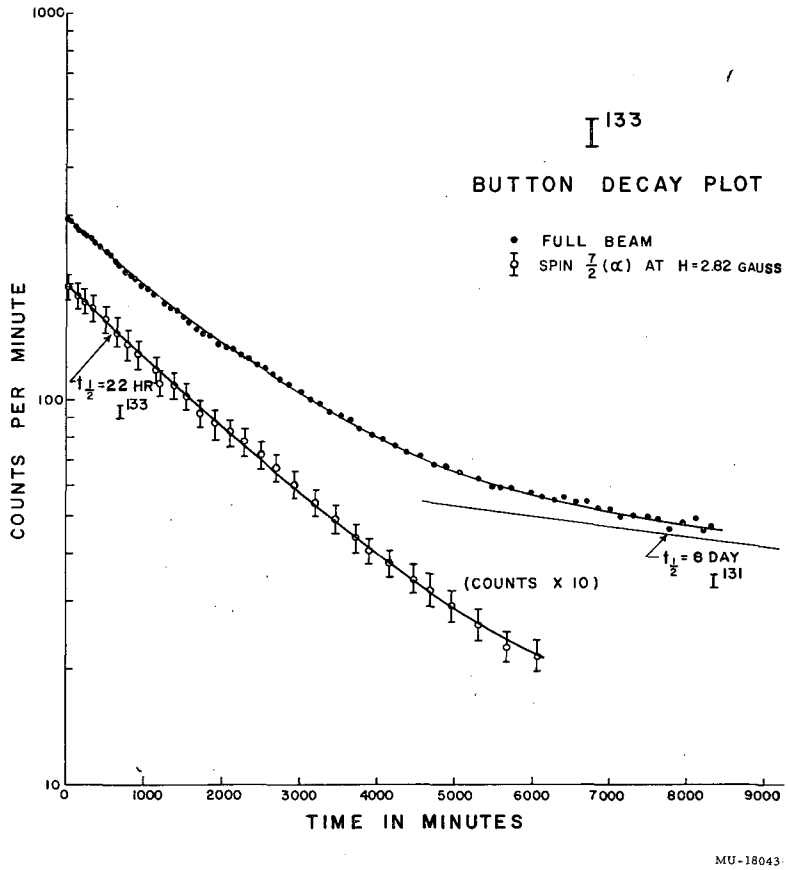

Fig. 37. Decay of full-beam and spin-7/2 (α) resonance buttons in I^{133}.

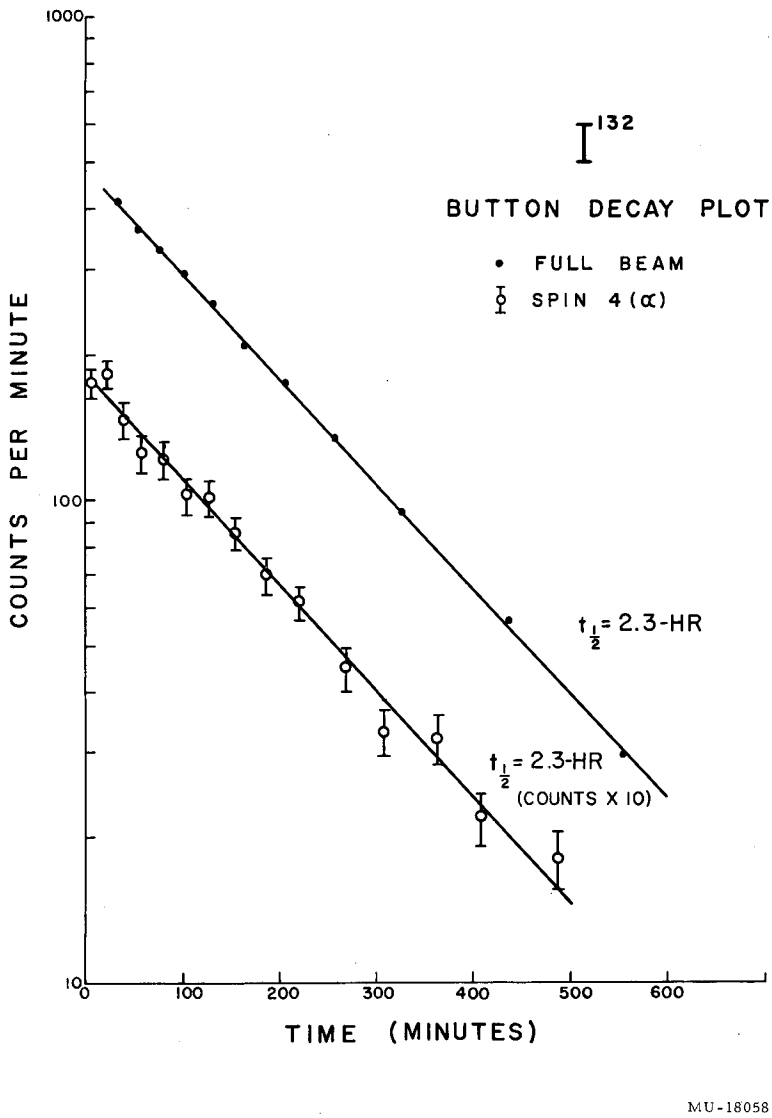

Fig. 38. Decay of full-beam and spin-4 (α) resonance buttons in I^{132}.

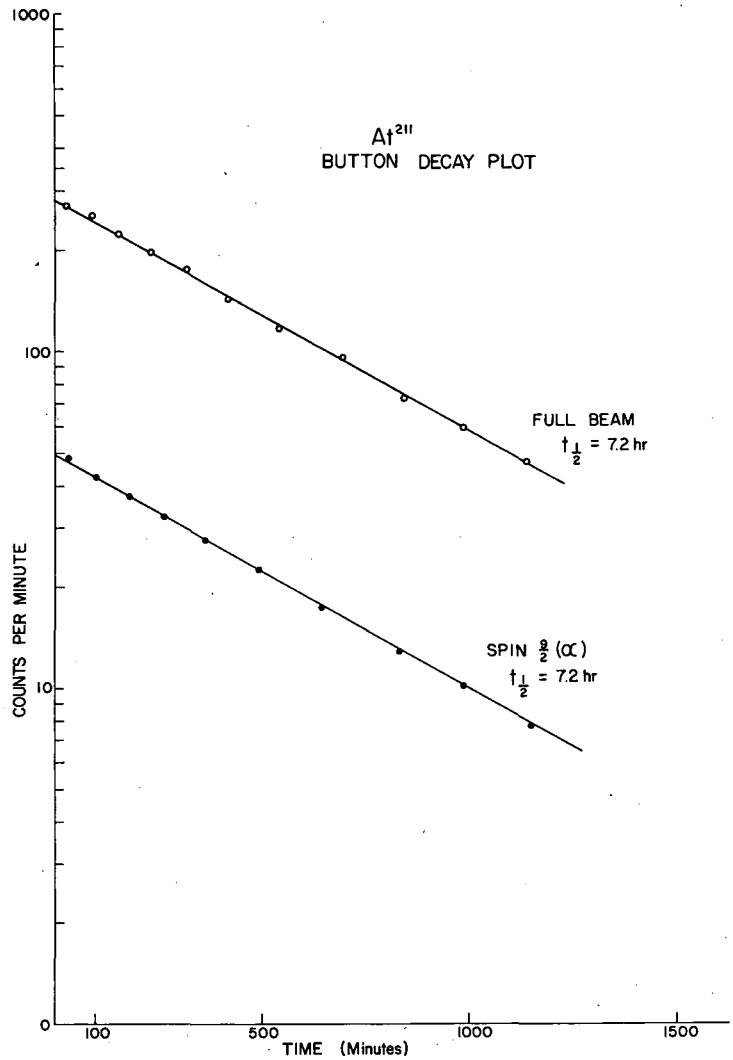

Mu-15558

Fig. 39. Decay of full-beam and spin-9/2 (α) resonance buttons in At^{211}.

APPENDIX B

Previous Experimental Observations On Iodine And Astatine

Among the early investigations of the atomic properties of iodine is listed the work of Turner who used an electrodeless discharge tube as a source of the iodine-arc spectrum.[23] In this spectrum he identified for the first time the $^2P_{1/2}$ and $^2P_{3/2}$ atomic states. In 1931, Evans[71] measured the ionization potential (10.454 v) for iodine and further analyzed the optical spectrum. Much of the iodine spectrum was reexamined by Murakawa in 1938.[72] A compilation of spectroscopic data by Moore[24] indicates that in recent years the entire iodine spectrum from 1200 A to 23,000 A has been reexamined by Kiess and Corliss (1200 A to 12,000 A) and by Plyler and Humphreys (12,000 A to 23,000 A) and also Eshbach and Fisher.[73] Over four hundred lines of the iodine spectrum have been classified.

The nuclear-spin value of I^{127} was determined by optical means by Tolansky in 1939.[74] Murakawa confirmed the value of $I = 5/2$, and reported the value of Q_{127} in 1955.[75] Optical spectroscopy has been used more recently by Onaka to observe the hyperfine-structure separation in the $^2P_{1/2}$ state of I^{127}.[70] His observations indicate that $\Delta\nu(^2P_{1/2}) = 0.670 \pm .07\ cm^{-1}$.

A great many investigations using magnetic-resonance and quadrupole-resonance techniques have been performed on iodine.

Some of the previous measurements have been referred to in Chapter VI. The spins of I^{127} and I^{129} were reaffirmed by Gordy in a microwave-absorption experiment.[76] The value of the magnetic moment, μ, of I^{127} was measured in 1958 by Pound[77] and the results compare closely with the more recent measurements by Walchi.[31]

The values of Q_{127} and Q_{129} were reported in 1947,[76] and in 1953 Livingston and Zeldes made a precise measurement of the ratio of Q_{129}/Q_{127}.[78] They obtained the value 0.701213 ± 0.000015 for this ratio, using a microwave spectrometer to observe quadrupole transitions.

The precise value of μ_{127} of I^{127} by Walchi is used as a standard in many of the recent measurements of the radioactive-iodine isotopes. Walchi obtained his values of μ_{127} = + 2.8090 ± 0.0004 nm and of μ_{129} = 2.6173 ± 0.0003 nm by comparing resonance frequencies in iodine to those for the proton, and then using $\mu(p)$ = 2.79268 nm from Sommer, Thomas, and Hipple.[79] A diamagnetic correction of 0.545% was also applied.

Other results of nuclear-magnetic-resonance experiments include the value of I, μ, and Q for I^{125} and the value of Q of I^{131} by Fletcher.[64] In addition, the value of I for I^{131} was measured by Livingston et al.[65]

In 1957, Bowers, Kamper, and Lustig measured the value of the electronic g factor in I^{127} [80] by a paramagnetic resonance experiment. They observed that the ratio of the g factor of

I^{127} to that of a free electron was $0.666225 \pm 1.5 \times 10^{-6}$. This value was used with a value of g_s for the electron of 2.0022920 to give g_J for iodine = 1.333977. This value was used in the results given in Chapter V.

The β and γ -ray studies of the iodine isotopes have been quite numerous and have succeeded in establishing the decay schemes for all of the iodine isotopes from I^{123} to I^{133}. Many of the references to these investigations are given in Chapter VI.

Attempts are presently being made to observe the optical emission and absorption spectrum of astatine, but to date the lines observed have not definitely been attributed to astatine.[81]

APPENDIX C

Relativistic Correction Factors

The relativistic correction factors $\mathcal{R}$ and $\mathcal{F}$ are obtained from Casimir.[22] They have the form:

$$\mathcal{R} = \frac{\ell(\ell+1)(2\ell+1)}{\rho(\rho^2-1)(4\rho^2-1)}\,[3k(k+1) - \rho^2 + 1]$$

and

$$\mathcal{F} = \frac{k(2k+1)(2\ell+1)}{\rho(4\rho^2-1)} = \frac{4j(j+1/2)(j+1)}{\rho(4\rho^2-1)}$$

where

$$j = \ell + 1/2 \text{ for } k = \ell + 1,$$

$$j = \ell - 1/2 \text{ for } k = -\ell,$$

and

$$\rho = \sqrt{k^2 - Z^2\alpha^2}\,.$$

For iodine, we have $j = \ell + 1/2$, $k = 2$, which gives the values:

$$\mathcal{R} = 1.128$$

$$\mathcal{F} = 1.061.$$

References

1. L. Dunoyer, Compt. Rend. 152, 594 (1911).
2. O. Stern, Z. Physik 7, 249 (1921).
3. Rabi, Zacharias, Millman, and Kusch, Phys. Rev. 53, 318 (1938).
4. Norman F. Ramsey, Nuclear Moments (John Wiley and Sons, Inc. New York, 1953).
5. Norman F. Ramsey, Molecular Beams (Oxford University Press, London, 1956).
6. William A. Nierenberg, Ann. Rev. Nuclear Sci. 7, 349 (1957).
7. Kenneth F. Smith, Molecular Beams (Methuen and Co., Ltd., London, 1955).
8. Kenneth F. Smith, Progr. Nuclear Phys. 6, 52 (1957).
9. A. Bohr, Phys. Rev. 81, 134 (1951).
10. A. Bohr, Kgl. Danske Videnskab. Selskab, Mat. - fys. Medd. 26, No. 14 (1952).
11. A. Bohr and B. R. Mottelson, Kgl. Danske Videnskab. Selskab, Mat.- fys. Medd. 27, No. 16, (1953).
12. S. G. Nilsson, Kgl. Danske Videnskab. Selskab, Mat-fys. Medd. 29, No. 16, (1955).
13. M. G. Mayer and J. H. D. Jensen, Elementary Theory of Nuclear Shell Structure (John Wiley and Sons, New York, 1955).

14. Davis, Feld, Zabel, and Zacharias, Phys. Rev. 76, 1076 (1949).

15. J. C. King and V. Jaccarino, Phys. Rev. 94, 1610 (1954).

16. Jaccarino, King, and Stroke, Phys. Rev. 94, 1798 (1954).

17. T. M. Green, Spins, Moments, and Hyperfine Structures of Some Bromine Isotopes, Thesis, UCRL-8730, June 1959.

18. J. R. Zacharias, Phys. Rev. 61, 270 (1942).

19. E. U. Condon and G. H. Shortley, The Theory of Atomic Spectra (University Press, Cambridge, 1951).

20. H. Kopfermann, Nuclear Moments (Academic Press, Inc, New York, 1958).

21. Charles Schwartz, Phys. Rev. 105, 173 (1957).

22. H. B. G. Casimir, On The Interaction Between Atomic Nuclei and Electrons (Teyler's Tweede Genootschap, Haarlem, 1936).

23. Louis A. Turner, Phys. Rev. 27, 397 (1926).

24. Charlotte E. Moore, Atomic Energy Levels, Vol. III, NBS-467 (National Bureau of Standards, Washington, D.C., 1958).

25. William A. Nierenberg, University of California Radiation Laboratory, Berkeley, private communication. Program description for IBM-653 computer.

26. Garvin, Green, Lipworth, and Nierenberg, Hyperfine Structure and Nuclear Moments of Bromine - 82, UCRL - 8680, March 9, 1959.

27. Lawrence L. Narino, Some Nuclear Properties of Bi^{206}, Tl^{200}, Tl^{202}, In^{109}, In^{110m}, and In^{111}. UCRL - 8721, April 1959.

28. E. Majorana, Nuovo cimento, 9, 43 (1932).

29. Garvin, Green, Lipworth, and Nierenberg, Phys. Rev. Lett. 1, 293 (1958).

30. R. A. Fisher, Statistical Methods for Research Workers (Oliver and Boyd, Edinburgh, 1958).

31. Walchi, Livingston, and Hebert, Phys. Rev. 82, 97 (1951).

32. R. Sternheimer, Phys. Rev. 84, 244 (1951).

33. R. Sternheimer, Phys. Rev. 86, 316 (1952).

34. Rabi, Zacharias, Millman, and Kusch, Phys. Rev. 53, 318 (1938).

35. Davis, Nagle, and Zacharias, Phys. Rev. 76, 1068 (1949).

36. Gilbert O. Brink, Nuclear Spins of Th^{197}, Th^{198m}, Th^{199}, and Th^{204}, Thesis, UCRL - 3642, June 1957.

37. M. Knudsen, Ann. Physik 28, 76 and 999 (1909).

38. Nierenberg, Hubbs, Hobson, and Silsbee, Phys. Rev. 96, 1450 (1954).

39. J. C. Hubbs and W. A. Nierenberg, Scintillation Detection of Very-Low-Energy Gamma Rays, UCRL - 3434, June 1956.

40. Sol Wexler, Revs. Modern Phys. 30, 402 (1958).

41. John C. Hubbs, The Spin, Hyperfine Splitting, and Magnetic Moment of Rubidium 81, Thesis, University of California, 1954.

42. Stang, Tucker, Banks, Doering, and Mills, Nucleonics 12, No. 8, 22 (1954).

43. Corson, Mackenzie, and Segre, Phys. Rev. 57, 1087 (1940).

44. Corson, Mackenzie, and Segre, Nature 159, 24 (1947).

45. Barton, Ghiorso, and Perlman, Radioactivity of Astatine Isotopes, UCRL - 670, Nov. 1950.

46. H. L. Garvin and E. Lipworth, Bull. Am. Phys. Soc., Ser. II, 2, 316 (1957).

47. Garvin, Green, Lipworth, and Nierenberg, Phys. Rev. 111, 534 (1958).

48. Garvin, Green, Lipworth, and Nierenberg, Phys. Rev. Lett., 1, 74 (1958).

49. Garvin, Green, Lipworth, Phys. Rev. Lett. 1, 292 (1958).

50. H. L. Garvin and E. Lipworth, Bull. Am. Phys. Soc., Ser. II, 4, 353 (1959).

51. P. F. A. Klinkenberg, Revs. Modern Phys. 24, 63 (1952).

52. J. E. Mack, Revs. Modern Phys. 22, 64 (1950).

53. S. A. Moskowski and C. J. Gallagher, Phys. Rev. 111, 1282 (1958).

54. L. W. Nordheim, Phys. Rev. 78, 294 (1950) and Revs. Modern Phys. 23, 322 (1951).

55. Way, Kundu, McGinnis, and Van Liesbout, Ann. Rev. Nuclear Sci. 6, 129 (1956).

56. Charles Schwartz, Phys. Rev. 94, 95 (1954).

57. M. L. Perlman and J. Welker, Phys. Rev. 95, 133 (1954).

58. Koerts, Macklin, Farrelly, Van Liesheut, and Wu, Phys. Rev. 98, 1230 (1955).

59. Jesse E. Sherwood, Bull. Am. Phys. Soc., Ser. II, 2, 344 (1957).

60. Benczer, Farrelly, Koerts, and Wu, Phys. Rev. 101, 1027 (1956).

61. J. E. Sherwood and S. J. Ovenshine, Bull. Am. Phys. Soc., Ser. II, 3, 371 (1958) and Phys. Rev. 114, 858 (1959).

62. R. S. Caird and A. C. G. Mitchell, Phys. Rev. 94, 412 (1954).

63. H. L. Finston and W. Bernstein, Phys. Rev. 96, 71 (1954).

64. P. C. Fletcher and E. Amble, Phys. Rev. 110, 536 (1957).

65. Livingston, Benjamin, Cox, and Gordy, Phys. Rev. 92, 1271 (1953).

66. Walter Gordy, Phys. Rev. 76, 139 (1949).

67. R. G. Barnes and W. K. Smith, Phys. Rev. 93, 95 (1954).

68. Kiyoshi Murakawa, Phys. Rev. 100, 1369 (1955).

69. G. F. Koster, Phys. Rev. 86, 148 (1952).

70. Ryumyo R. Onaka, Phys. Rev. 106, 1178 (1957).

71. S. F. Evans, Proc. Roy. Soc. (London), A, 133, 417 (1931).

72. Kiyoshi Murakawa, Z. Phys. 109, 171 (1938).

73. F. E. Eshbach and R. A. Fischer, J. Opt. Soc. Am. 44, 868 (1954); C. C. Kiess and C. H. Corliss, Nat. Bur. Standards (U.S.), unpublished work.

74. S. Tolansky, Proc. Roy. Soc. (London), A, 170, 205 (1939).

75. Kiyoshi Murakawa, Phys. Rev. 100, 1369 (1955).

76. Gordy, Smith, and Simmons, Phys. Rev. 76, 249 (1947).

77. R. V. Pound, Phys. Rev. 73 523 (1948) and Phys. Rev. 74, 228 (1948).

78. R. Livingston and H. Feldes, Phys. Rev. 90, 609 (1953).

79. Sommer, Thomas, Ripple, Phys. Rev. 80, 487 (1950).

80. Bowers, Kamper, and Lustig, Proc. Roy. Soc. (London), B, Vol. 70, 445 (1957).

81. Ralph D. McLaughlin, Lawrence Radiation Laboratory, Berkeley, California, private communication.

This report was prepared as an account of Government sponsored work. Neither the United States, nor the Commission, nor any person acting on behalf of the Commission:

A. Makes any warranty or representation, expressed or implied, with respect to the accuracy, completeness, or usefulness of the information contained in this report, or that the use of any information, apparatus, method, or process disclosed in this report may not infringe privately owned rights; or

B. Assumes any liabilities with respect to the use of, or for damages resulting from the use of any information, apparatus, method, or process disclosed in this report.

As used in the above, "person acting on behalf of the Commission" includes any employee or contractor of the Commission, or employee of such contractor, to the extent that such employee or contractor of the Commission, or employee of such contractor prepares, disseminates, or provides access to, any information pursuant to his employment or contract with the Commission, or his employment with such contractor.